Title:

Non-invasive multi-channel electrophysiology of the human spinal cord – assessing somatosensory processing from periphery to cortex

Author names and affiliations:
Birgit Nierula[1], Tilman Stephani[2,3,4], Merve Kaptan[1,4], André Mouraux[5], Burkhard Maess[6], Arno Villringer[3], Gabriel Curio[7], Vadim V. Nikulin[2,3,7*], Falk Eippert[1*]

1. Max Planck Research Group Pain Perception, Max Planck Institute for Human Cognitive and Brain Sciences, 04103 Leipzig, Germany
2. Research Group Neural Interactions and Dynamics, Department of Neurology, Max Planck Institute for Human Cognitive and Brain Sciences, 04103 Leipzig, Germany
3. Department of Neurology, Max Planck Institute for Human Cognitive and Brain Sciences, 04103 Leipzig, Germany
4. International Max Planck Research School NeuroCom, 04103 Leipzig, Germany
5. Institute of Neuroscience, Université Catholique de Louvain, 1200 Brussels, Belgium
6. Methods and Development Group Brain Networks, Max Planck Institute for Human Cognitive and Brain Sciences, 04103 Leipzig, Germany
7. Department of Neurology, Charité University Medicine, 12200 Berlin, Germany
*. These authors contributed equally.

Corresponding author email address: Birgit Nierula (nierula@cbs.mpg.de), Falk Eippert (eippert@cbs.mpg.de), Vadim V. Nikulin (nikulin@cbs.mpg.de)

Author contributions listed alphabetically according to CRediT taxonomy (https://credit.niso.org):
Conceptualization: FE, BN, VVN.
Data curation: BN.
Formal analysis: MK, BN, TS.
Funding acquisition: FE.
Investigation: BN.
Methodology: GC, FE, AM, BN, VVN.
Project administration: FE, BN.
Resources: FE, VVN, AV.
Software: MK, BN, TS.
Supervision: FE, VVN.
Visualization: BN.
Writing – original draft: FE, BN.
Writing – review & editing: GC, FE, MK, BM, AM, BN, TS, VVN, AV.

Abstract

The spinal cord is of fundamental importance for somatosensory processing and plays a significant role in various pathologies, such as chronic pain. However, knowledge on spinal cord processing in humans is limited due to the vast technical challenges involved in its investigation via non-invasive recording approaches. Here, we aim to address these challenges by developing an electrophysiological approach – based on a high-density electrode-montage – that allows for characterizing spinal cord somatosensory evoked potentials (SEPs) and combining this with concurrent recordings of the spinal cord's input (peripheral nerve action potentials) and output (SEPs in brainstem and cortex). In two separate experiments, we first methodologically validate the approach (including replication and robustness analyses) and then assess its application in the context of a neuroscientific question (integrative processes along the neural hierarchy). Critically, we demonstrate the benefits of multi-channel recordings in terms of enhancing sensitivity via spatial filtering, which also allows for obtaining spinal cord SEPs at the single-trial level. We make use of this approach to demonstrate the feasibility of recording spinal cord SEPs in low-signal scenarios (single-digit stimulation) and – most importantly – to provide evidence for bottom-up signal integration already at the level of the spinal cord. Taken together, our approach of concurrent multi-channel recordings of evoked responses along the neural hierarchy allows for a comprehensive assessment of the functional architecture of somatosensory processing at a millisecond timescale.

Introduction

The spinal cord is an important interface between the body and the brain (Hochman, 2007) that not only harbors the motor neurons directly innervating the skeletal muscles but it is also the first processing stage of the central nervous system for somatosensory information conveyed along the peripheral nerves. Traditional depictions of the spinal cord portray it mainly as a relay station, yet recent studies paint a more nuanced picture, for example in the somatosensory domain, where a high degree of neuronal complexity and organization has been delineated (Abraira et al., 2017; Häring et al., 2018; Li et al., 2011). Despite these advances in basic research and the spinal cord's involvement in numerous diseases, such as chronic pain (Kuner & Flor, 2017) or multiple sclerosis (Ciccarelli et al., 2019), knowledge on processing in the human spinal cord is still very limited.

A large body of knowledge on spinal cord processing has been generated from research in animal models, where invasive recording techniques – such as multi-electrode recordings (McPherson & Bandres, 2021) or calcium imaging (Ran et al., 2016) – allow detailed and mechanistic insights into processes occurring at the micro- and mesoscale. In human neuroscience, approaches such as reflex assessments (e.g., via the H-reflex (Schieppati, 1987) or the nociceptive flexion reflex (Sandrini et al., 2005)) allow for very useful, but only indirect assessments of the processes occurring within the spinal cord. More direct assessments of human spinal cord activity would thus be desirable, yet several factors make the spinal cord a very challenging target for non-invasive neuroimaging techniques: the spinal cord has a small diameter, is located deep in the body in close proximity to inner organs such as the heart and lungs, and is protected by the vertebral column and several muscle layers.

Consequently, compared to the multitude of methods for non-invasively assessing human brain function, there is a lack of well-established and readily available approaches to interrogate human spinal cord function. Functional magnetic resonance imaging (fMRI) of the human spinal cord was established ~25 years ago (Yoshizawa et al., 1996) and has since provided valuable insights into spinal processing in health and disease (Kinany et al., 2022; Landelle et al., 2021; Wheeler-Kingshott et al., 2014). However, not only is spinal cord fMRI technically very challenging (Cohen-Adad, 2017) and performed by only a small number of groups worldwide, but fMRI in general is fundamentally limited by its coarse temporal resolution (in the order of seconds) and its indirect link to neuronal activity due to neurovascular coupling. Conversely, magnetospinography (MSG) based on super-conducting quantum interference devices (SQUIDs) is a non-invasive method with high temporal resolution that directly measures the magnetic fields generated by the synchronized activity of neuronal populations in the spinal cord. Since its inception ~30 years ago (Curio et al., 1991), however, no commercially available systems have been developed and – to our knowledge – currently only one group is pursuing this very promising approach (Akaza et al., 2021; Hashimoto et al., 2022; Sumiya et al., 2017; for a recent MSG approach based on optically pumped magnetometers, see Mardell et al., 2022).

Compared to MSG and spinal cord fMRI – which require major investments in large-scale equipment and are technically very challenging – there is a large body of literature on non-invasive electrospinography (ESG) for recording somatosensory evoked potentials (SEP) from the spinal

cord of healthy human volunteers via surface electrodes placed on the neck or back of a participant. This line of research started in the late 1960s and early 1970s (Cracco, 1972, 1973; Jones, 1977; Liberson et al., 1966; Matthews et al., 1974) and reached its publication peak in the 1980s. The majority of these studies were not focused on basic neuroscientific aspects but were motivated by the development of SEPs as diagnostic or monitoring biomarkers for clinical use (for review, see Cruccu et al., 2008; Mauguière, 2000). Typically, these studies would stimulate mixed nerves at the wrist (median nerve) or the ankle (tibial nerve) in order to elicit spinal cord SEPs with high amplitudes and record them using a simple setup with one electrode placed at an anatomically defined location on the dorsal neck or the back. Using such approaches, a canonical set of early potentials with a post-synaptic origin in the dorsal horn of the spinal cord has been reported (Delbeke et al., 1978; Desmedt & Cheron, 1981a; Desmedt & Huy, 1984; Emerson et al., 1984; Ratto et al., 1983; Yamada et al., 1980): spinal SEPs present as negative deflection in the cervical part 13 ms after stimulation (N13) and in the lumbar part 22 ms after stimulation (N22). While thus providing a direct window into processing in the human spinal cord, in the last decade only very few studies recorded such spinal cord SEPs non-invasively in healthy human volunteers to our knowledge (Boehme et al., 2019; Chander et al., 2022; Di Pietro et al., 2021; Fabbrini et al., 2022; Rocchi et al., 2018), despite considerable improvements of both recording capabilities and processing techniques for non-invasive neurophysiological data.

Here, we aimed to build upon this body of literature by developing a non-invasive method for direct recordings of spinal cord potentials with high sensitivity in order to allow for a comprehensive characterization of spinal cord processing. To this end, we i) recorded both the input to (peripheral nerve action potentials, NAPs) and the output from the spinal cord (brainstem and cortical SEPs), ii) recorded spinal cord SEPs with high temporal precision (10 kHz) and extensive spatial coverage (multi-channel montage of 39 surface electrodes placed over the neck and trunk in two electrode grids), iii) used artifact-correction techniques from electroencephalography (EEG) to increase the signal-to-noise ratio in spinal cord signals and iv) employed multi-variate analysis approaches that allowed for increased robustness as well as extraction of single-trial spinal cord SEPs.

This approach was employed in two studies (Experiment 1: N=36; Experiment 2: N=24), where we recorded responses from the peripheral nerves, the spinal cord, the brainstem, and the cortex to electrical stimulation of the upper and lower limb (see Figure 1 for an overview of the two studies and the electrode montage). In Experiment 1 – which served to methodologically validate our approach – we employed mixed nerve stimulation of the median nerve (at the wrist) and the tibial nerve (at the ankle) to elicit robust SEPs with high amplitude, aiming to i) replicate previously observed spinal SEPs together with the input to (periphery) and output from the spinal cord (brainstem, cortex), ii) characterize the spinal cord SEPs spatially and temporally, iii) enhance the sensitivity of spinal cord SEPs by making use of the multi-electrode setup, and iv) assess the robustness of spinal responses at the individual participant and group level. In Experiment 2 – which served to replicate spinal cord results from Experiment 1 and to investigate a fundamental neuroscientific question – we additionally electrically stimulated sensory branches of the median nerve at the index and middle fingers (and sensory branches of the tibial nerve at the first and

second toes), either individually or simultaneously, aiming to i) assess the potential of our approach to also reliably record spinal SEPs that have a lower signal-to-noise ratio, ii) investigate whether lower-level responses predict higher-level responses along the somatosensory processing hierarchy, and, most importantly, iii) investigate whether integrative processes already occur at the level of the spinal cord.

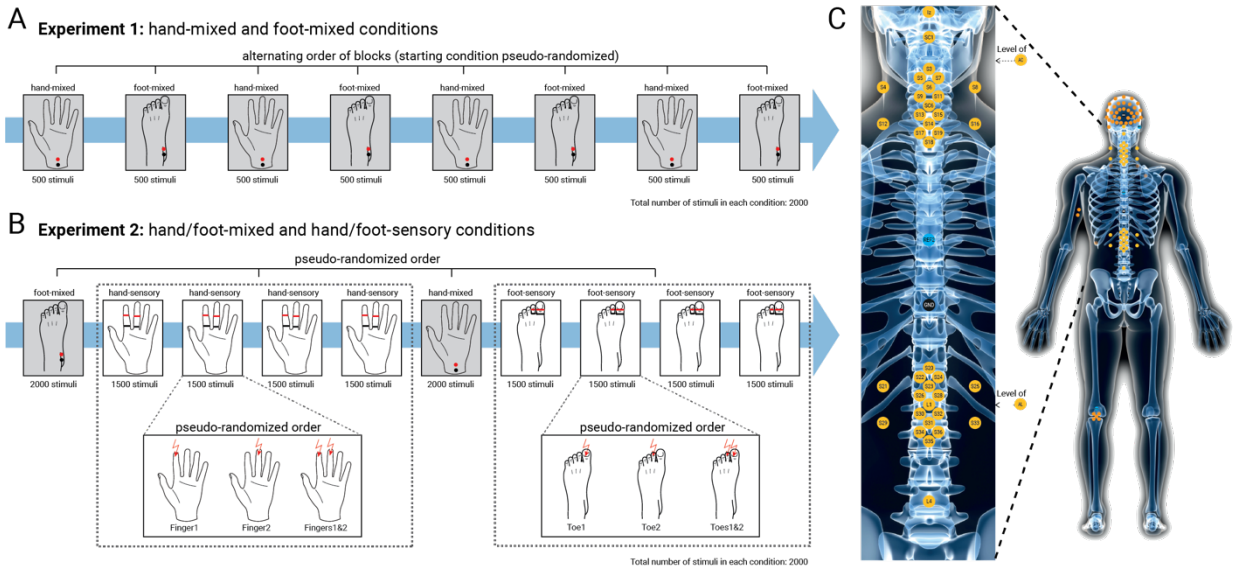

***Figure 1. Overview of experimental conditions and spinal cord recording setup**. **A)** In Experiment 1, electrical mixed nerve stimulation was applied just above the individual motor threshold to the left median nerve at the wrist (hand-mixed) and to the left tibial nerve at the ankle (foot-mixed). Four hand-mixed and four foot-mixed blocks of 500 stimuli each (delivered at an average frequency of ~1.3 Hz) were presented in alternating order. **B)** In Experiment 2, electrical mixed nerve stimulation was applied to the same location as in Experiment 1 in blocks of 2000 stimuli. In addition, sensory nerve stimulation was applied to the left index and middle finger (hand-sensory) and to the first and second toe (foot-sensory) at an intensity of three times the sensory threshold. Sensory stimulation blocks were separated into 4 consecutive blocks of the same stimulation type (either hand-sensory or foot-sensory) and each block consisted of 1500 stimuli (500 finger1/toe1, 500 finger2/toe2, and 500 fingers1&2/toes1&2, in pseudo-random order). The average stimulation frequency in Experiment 2 was ~3.9 Hz. **C)** Across both experiments, stimulus-locked responses were recorded at the level of the peripheral nerves, the spinal cord, and the brain. Peripheral NAPs were recorded from the ipsilateral axilla and Erb's point for median nerve stimulation and from the ipsilateral popliteal fossa (cluster of 5 electrodes) and the cauda equina for tibial nerve stimulation. Spinal cord SEPs were recorded with a montage of 37 dorsal and 2 ventral electrodes, which had a cervical and a lumbar focus: around an anatomical target electrode (placed over the spinous process of either the 6th cervical vertebra or the 1st lumbar vertebra), 17 electrodes were placed in a grid with distances optimized for capturing the spatial distribution of the spinal signal. Additionally, the following electrodes were contained in the spinal montage: one over the inion, one over the first cervical vertebra, one over the spinous process of the 4th lumbar vertebra, and two ventral electrodes (AC located supra-glottically and AL located supra-umbilically). All electrodes of the spinal montage were referenced to an electrode placed over the spinous process of the 6th thoracic vertebra. Cortical SEPs were recorded with a 64-channel EEG setup in Experiment 1 (39 channels in Experiment 2).*

Results

Experiment 1: Somatosensory responses along the neural hierarchy following mixed nerve stimulation

As a first objective, we aimed to replicate previously reported somatosensory responses along the neural hierarchy, with a special focus on the spinal cord. Towards this end, we employed mixed nerve stimulation at the upper and lower limb (conditions: hand-mixed and foot-mixed) and recorded peripheral NAPs as well as SEPs from the spinal cord, brainstem and cortex. In the hand-mixed condition, we extracted the peripheral N6 (origin: median nerve; recording site: axilla), the peripheral N9 (origin: brachial plexus; recording site: Erb's point), the spinal N13 (origin: dorsal horn; recording site: spinous process of 6th cervical vertebra), the brainstem N14 (likely origin: cuneate nucleus; recording site: 1st cervical vertebra) and the cortical N20 (origin: primary somatosensory cortex; recording site: CP4). In the foot-mixed condition, we extracted the peripheral N8 (origin: tibial nerve; recording site: popliteal fossa), the spinal N22 (origin: dorsal horn; recording site: spinous process of the 1st lumbar vertebra), the brainstem N30 (likely origin: gracile nucleus; recording site: 4 cm above the spinous process of the 6th vertebra) and the cortical P40 (origin: primary somatosensory cortex; recording site: Cz). In order to obtain spinal cord SEPs with high sensitivity, we performed a thorough heart-artifact correction of the ESG data, removed line noise with a notch filter, band-pass-filtered the data between 30 and 400 Hz, removed noisy trials and channels, re-referenced the data to a ventral cervical or lumbar channel, and computed SEPs from the remaining trials (see Method sections for more details).

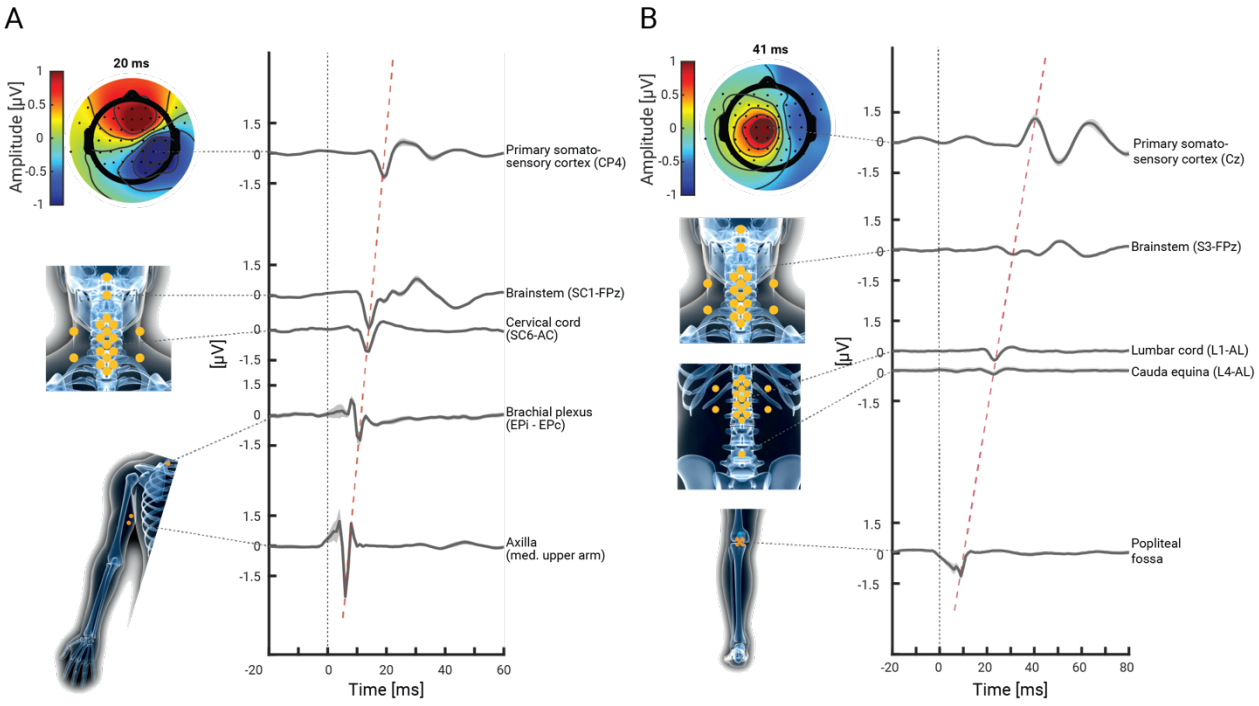

Figure 2. Grand average NAPs and SEPs along the somatosensory processing hierarchy. *Group-average responses in the hand-mixed* ***(A)*** *and the foot-mixed* ***(B)*** *conditions of Experiment 1, with shaded error-bands depicting the*

standard error of the mean across the group (N=36). In each panel, the bottom two traces depict peripheral NAPs, the middle trace depicts spinal cord SEPs (referenced ventrally) and the top two traces depict brainstem and cortical SEPs, respectively. The grey dashed lines point to the electrode from which the respective trace was obtained, the isopotential plots display the spatial topography of the early cortical SEP and the red dashed line depicts the temporal progression of the signal along the hierarchy.

At all recording sites, we replicated previously observed somatosensory responses with the expected latencies (Table 1). Grand-average time-courses at the group-level (N=36) are depicted in Figure 2 (with an additional recording of cauda equina NAPs) and show the temporal progression of the signal along the neural hierarchy. The amplitudes of all potentials were highly significant at the group level and exhibited consistently large effect sizes (Table 1). To furthermore ensure the robustness of these results, we replicated them in Experiment 2 (N=24; Supplementary Table 1). Altogether, these results give a comprehensive overview of evoked potentials along the entire somatosensory processing hierarchy following electrical stimulation of a hand and a foot nerve.

Table 1. *Group-level descriptive statistics for SEP- and peripheral NAP-amplitudes, latencies and SNR (mean and standard error of the mean) and one-sample t-test of SEP- and peripheral NAP-amplitudes against zero in the hand-mixed and foot-mixed conditions of Experiment 1 (N = 36). Note that the brainstem analysis (N14 / N30) is based on 30 participants only due to a technical problem (see Methods section; vr = ventral reference, tr = thoracic reference, CCA – canonical correlation analysis, SEP = somatosensory evoked potential, NAP = nerve action potential, # = number of participants in which potential was visible at the individual level, SNR = signal-to-noise ratio).*

SEP / NAP	#	Latency [ms]	Amplitude [µV / a.u.]	SNR	tstat	p	95%-CI	Cohen's d
Mixed median nerve stimulation (hand-mixed)								
N6	32	6.22 ± 0.09	-3.22 ± 0.55	14.09 ± 2.3	-5.89	<0.001	[-4.33; 2.11]	-0.98
N9	35	10.56 ± 0.15	-2.41 ± 0.21	8.8 ± 1.41	-11.55	<0.001	[-2.83; -1.99]	-1.92
N13 (tr)	36	13.25 ± 0.18	-0.85 ± 0.05	9.48 ± 1.16	-15.75	<0.001	[-0.96; -0.74]	-2.63
N13 (vr)	36	13.61 ± 0.17	-1.40 ± 0.08	17.38 ± 3.4	-17.01	<0.001	[-1.56; -1.23]	-2.84
N13 (CCA)	36	13.28 ± 0.17	-0.47 ± 0.03	21.58 ± 2.93	-16.93	<0.001	[-0.53; -0.42]	-2.82
N14	30	14.30 ± 0.19	-2.34 ± 0.14	24.19 ± 3.04	-16.95	<0.001	[-2.62; -2.06]	-3.09
N20 (CCA)	36	19.81 ± 0.20	-1.41 ± 0.06	23.66 ± 2.41	-21.85	<0.001	[-1.54; -1.28]	-3.64
Mixed tibial nerve stimulation (foot-mixed)								
N8	34	9.28 ± 0.16	-1.58 ± 0.18	10.23 ± 1.72	-8.64	<0.001	[-1.95; -1.21]	-1.44
N22 (tr)	36	23.83 ± 0.29	-0.80 ± 0.08	9.79 ± 1.72	-9.54	<0.001	[-0.97; -0.63]	-1.59
N22 (vr)	36	23.67 ± 0.35	-0.61 ± 0.06	14.14 ± 2.42	-10.42	<0.001	[-0.72; -0.49]	-1.74
N22 (CCA)	36	23.75 ± 0.29	-0.62 ± 0.06	31.28 ± 5.96	-10.74	<0.001	[-0.73; -0.50]	-1.79
N30	30	32.13 ± 0.43	-0.53 ± 0.04	6.57 ± 1.08	-13.29	<0.001	[-0.61; -0.45]	-2.43
P40 (CCA)	36	40.86 ± 0.38	1.42 ± 0.08	21.22 ± 2.07	18.17	<0.001	[1.26; 1.58]	3.03

Experiment 1: Detailed characterization of spinal cord SEPs

Having provided an overview of somatosensory responses from periphery to cortex, we now turn to characterizing the spinal potentials in more detail. First, when looking at the time-course of the potentials obtained from single, anatomically-defined target electrodes (hand-mixed: over the spinous process of the 6th cervical vertebra; foot-mixed: over the spinous process of the 1st lumbar vertebra; reference for both over the spinous process of the 6th thoracic vertebra), a tri-phasic shape

with an initial positive deflection, a main negative deflection (at 13 ms and 24 ms, respectively) and a slowly decaying late positive deflection are visible (red trace in Figure 3B and 3G). Second, the spatial topography at the peak latency (Figure 3C and 3F) shows a central distribution with a radial dipole that is limited to either the cervical or the lumbar electrode grid. Third, grand-average time-frequency plots show that the cervical potential has a frequency between approximately 50 Hz and 320 Hz at the cervical (channel SC6-TH6) and between 50 Hz and 250 Hz at the lumbar level (channel L1-TH6).

Finally, we aimed to enhance the sensitivity of our approach for detecting spinal cord SEPs by making use of the multi-channel setup. A first motivation for this is already apparent when looking at the grand average isopotential plot of the cervical N13 peak (Figure 3C), where one can see that the anatomically-defined target channel, which is located over the 6th cervical vertebra (and displayed in red at the center of the cervical electrode patch), might not be the optimal channel in the patch to extract the strongest deflection of the cervical N13, which is slightly shifted rostrally. This is similar for the lumbar N22, which has the target channel at the first lumbar vertebra (Figure 3F) and where the peak of the spatial distribution exhibits a slight caudal shift. Considering that these are group-level results and that individual spatial shifts will be even stronger, this indicates a necessity of having a grid of electrodes in order to be able to detect heterogeneity in source location and orientation. In order to include the signal from all channels of the cervical or lumbar patch and to allow to use different channel combinations per participant (and thereby account for inter-participant variability of the optimal channel), we applied a variant of canonical correlation analysis (CCA) to the preprocessed data of the cervical or lumbar ESG channel patch. CCA is a multivariate method that takes information from all sensors of interest into account and that has been used for single-trial extraction of early SEP at the cortical level (Fedele et al., 2013; Stephani et al., 2020, 2021, 2022; Waterstraat et al., 2015). By finding spatial filters that maximize the correlation between two multivariate datasets (in our case the single SEP trials and the averaged SEP), it computes multiple orthogonal projections. For each participant, we selected the strongest CCA projection with a clear peak at the corresponding potential latency and with a pattern that displayed the expected dipole orientation. The resulting cervical N13 and lumbar N22 were similar in shape and latency but clearly exceeded noise level compared to the sensor-space signal (black trace in Figure 3B and 3G, time courses are normalized for comparison). Most importantly, this procedure enhanced the signal-to-noise ratio of the evoked responses in a way that allowed the extraction of spinal cord cervical and lumbar SEPs at the single-trial level in all participants: Figures 3A and 3H show single-participant CCA-cleaned SEPs at single-trial level, comparing the CCA projected data (right subpanel) with single-electrode data (left subpanel), clearly demonstrating the increase in signal-to-noise level in CCA-cleaned data. Our results thus indicate that taking the information from many channels into account provides a clear benefit for extracting spinal cord SEP amplitudes.

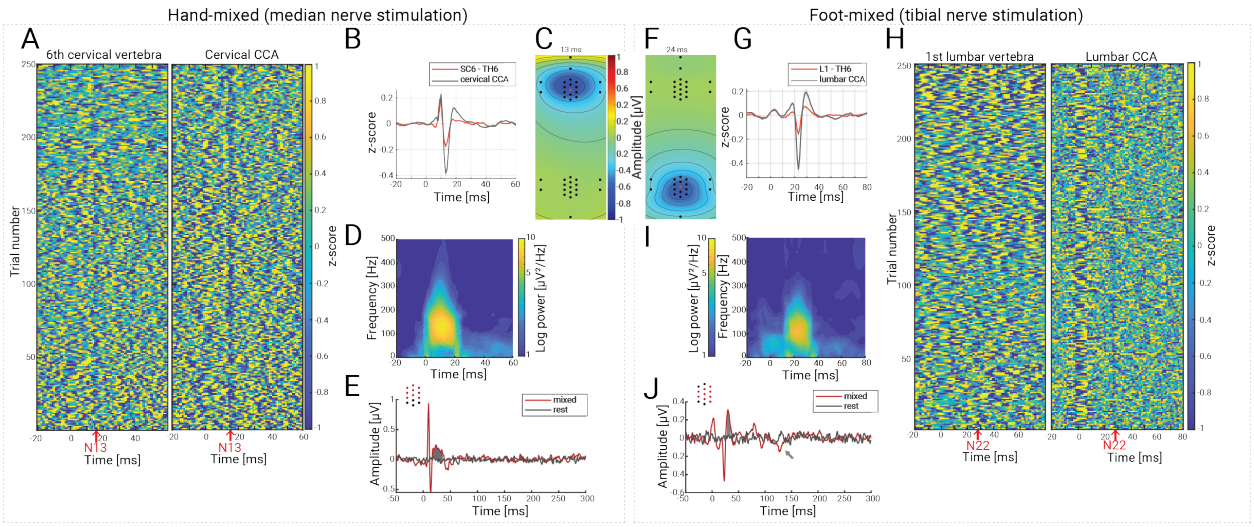

Figure 3. Spatiotemporal characterization of cervical and lumbar spinal cord potentials. *Panels **A-E** depict responses in the hand-mixed conditions and Panels **F-J** depict responses in the foot-mixed condition. **(A)** and **(H)** depict 250 single trials of evoked responses (vertical axis) of one representative participant (sub-011): the left subpanel shows responses obtained from an anatomically-defined electrode (hand-mixed: 6th cervical vertebra; foot-mixed: 1st lumbar vertebra) and the right plot subpanel shows responses obtained after CCA. The red arrow shows the timepoint of the expected SEP (hand-mixed: N13; foot-mixed: N22). Note that the negative deflection of the N13/N22 is hardly visible at the single-trial level in the single-electrode data, but clearly apparent after CCA. **(B)** and **(G)**: Grand-average SEPs across the group obtained from an anatomically-defined electrode (hand-mixed: 6th cervical vertebra; foot-mixed: 1st lumbar vertebra; red trace; both with thoracic reference over the spinous process of the 6th thoracic vertebra (TH6)) or after CCA (black trace), with both signals z-scored for comparison. Note the clear amplitude enhancement of the N13 and N22 after CCA. **(C)** and **(F)**: Grand-average isopotential plots (over all dorsally located spinal channels) in the hand-mixed condition at the peak of the N13 **(C)**, and in the foot-mixed condition at the peak of the N22 **(F)**. **(D)** and **(I)**: Grand-average evoked time frequency plots in the hand-mixed condition and the foot-mixed condition. **(E)** and **(J)** display results from cluster-based permutation testing for investigating potentials that occur after the N13 or N24. Depicted is the grand-average trace over all participants in the stimulation condition (hand-mixed / foot-mixed; red trace) and in simulated epochs from rest data (black trace). The plotted signal is an average over all channels that are part of the identified cluster and which are also displayed as red dots on the top left. The gray areas identify the time range in which stimulation and rest data are statistically different: this occurs at 17-35 ms in the cervical data and at 28-35 ms in the lumbar data. In the lumbar data, the gray arrow indicates an additional late potential that is depicted in Supplementary Figure 1, but which did not replicate in Experiment 2.*

Experiment 1: SEP components in the cervical and lumbar spinal cord that occur later than the N13 or the N22

The large majority of previous studies have focused on the properties of the classical spinal SEPs – the N13 and N22 – and have typically not investigated later SEP components at the spinal level. However, considering recent findings on the complexity of somatosensory processing in the dorsal horn (Abraira et al., 2017), we wanted to assess whether we could detect SEP components that occur later than the early N13 or N22 components. We therefore followed the same preprocessing steps for ESG data, but now filtered with a broader frequency band (5 Hz to 400 Hz), since later components could have lower frequency content. Using resting-state data from the same

participants obtained at the very beginning of Experiment 1, we created a surrogate time series with the same stimulation sequence that we preprocessed in the same way. Over a region of interest consisting of the three central columns of the cervical or lumbar electrode grid, we systematically compared the signal from stimulation-runs and from rest-runs in the time window from 0 ms (stimulation onset) to 600 ms using a cluster-based permutation test (in space and time) and here focused on responses occurring after the above-reported early potentials (the cluster-based permutation test also identified the N13 and N22, but these are ignored here). In the hand-mixed condition, we identified a cervical cluster directly after the N13 component between 17 ms and 35 ms (Monte Carlo corrected p-value p_{mcc} = 0.001; Figure 2E) that has higher activity during stimulation than during rest. In the foot-mixed condition, we identified two lumbar clusters: i) a positive cluster directly after the N22 component between 28 ms and 35 ms (p_{mcc} = 0.002; Figure 3J) and ii) a negative cluster between 126 and 132 ms (p_{mcc} = 0.017; Supplementary Figure 1). We also used data from Experiment 2 in order to replicate these results and found that the cervical cluster and the positive lumbar cluster were replicated in this independent sample, but that this was not the case for the negative lumbar cluster (see Supplementary Information section III). Taken together, these results provide evidence for SEP components that occur later than the initial activity in the spinal cord.

Experiment 2: SEP components in the cervical and lumbar spinal cord following mixed and sensory nerve stimulation

Electrical mixed nerve stimulation at the wrist or ankle – as employed in Experiment 1 – produces the strongest SEP response in the somatosensory system, but it is not an ecologically valid type of stimulation (e.g., due to antidromic conduction). To get one step closer towards natural stimulation, we additionally stimulated purely sensory nerve fibers in Experiment 2, which typically produces signals with a temporal delay and a lower signal-to-noise ratio and results in SEPs more difficult to dissociate from biological and non-biological noise (Pratt et al., 1979; Pratt & Starr, 1981). More specifically, in Experiment 2 we i) repeated electrical mixed nerve stimulation as in Experiment 1 and ii) electrically stimulated sensory nerve fibers in two digits (left index and middle finger or left first and second toe) either alone or simultaneously.

First, we replicated the main findings of Experiment 1 in terms of latency and amplitude of potentials to mixed nerve stimulation along the neuraxis (Supplementary Table 1). Second, using the same anatomically-defined electrode positions as in Experiment 1 (spinous process of the 6th cervical or the 1st lumbar vertebra) we observed spinal SEPs to sensory nerve stimulation, though now with an increased latency and reduced amplitude, SNR and effect size; this pattern of results was also observed in peripheral NAPs and cortical SEPs for both finger and toe stimulation (Table 2). Similar to the mixed nerve results, applying CCA resulted in a clear enhancement of sensory nerve SNR.

Table 2. *Group-level descriptive statistics for SEP- and peripheral NAP -amplitudes, latencies and SNR (mean and standard error of the mean) and one-sample t-test of SEP- and peripheral NAP -amplitudes against zero in all hand-sensory and foot-sensory conditions of Experiment 2 (N=24, vr = ventral reference, tr = thoracic reference, CCA –*

canonical correlation analysis, SEP = somatosensory evoked potential, NAP = nerve action potential, # = number of participants in which potential was visible at the individual level, SNR = signal-to-noise ratio).

SEP / NAP	#	Latency [ms]	Amplitude [µV / a.u.]	SNR	tstat	p	95%-CI	Cohen's d
Sensory median nerve stimulation (hand-sensory)								
		Index finger (finger1)						
N6	23	10.29 ± 0.15	-0.34 ± 0.04	9.90 ± 1.82	-8.32	<0.001	[-0.43; -0.26]	-1.7
N13 (tr)	21	18.13 ± 0.26	-0.19 ± 0.04	2.36 ± 0.35	-5.02	<0.001	[-0.26; -0.11]	-1.03
N13 (vr)	23	18.13 ± 0.24	-0.25 ± 0.04	3.33 ± 0.59	-6.38	<0.001	[-0.33; -0.17]	-1.30
N13 (CCA)	21	18.17 ± 0.20	-0.09 ± 0.01	3.50 ± 0.68	-5.71	<0.001	[-0.12; -0.05]	-1.16
N20 (CCA)	24	23.79 ± 0.23	-0.34 ± 0.04	17.08 ± 3.73	-9.16	<0.001	[-0.41; -0.26]	-1.87
		Middle finger (finger2)						
N6	23	10.17 ± 0.14	-0.41 ± 0.05	9.42 ± 1.56	-8.91	<0.001	[-0.50; -0.31]	-1.82
N13 (tr)	23	17.92 ± 0.28	-0.24 ± 0.06	2.28 ± 0.45	-3.84	0.001	[-0.38; -0.11]	-0.78
N13 (vr)	23	17.75 ± 0.25	-0.42 ± 0.06	3.31 ± 0.43	-7.35	<0.001	[-0.53; -0.30]	-1.50
N13 (CCA)	24	17.79 ± 0.29	-0.12 ± 0.01	4.90 ± 1.24	-8.60	<0.001	[-0.15; -0.09]	-1.76
N20 (CCA)	24	23.71 ± 0.26	-0.41 ± 0.04	22.29 ± 6.40	-9.59	<0.001	[-0.50; -0.32]	-1.96
		Index and middle finger (fingers1&2)						
N6	23	10.13 ± 0.13	-0.76 ± 0.08	11.34 ± 1.84	-9.51	<0.001	[-0.93; -0.60]	-1.94
N13 (tr)	22	17.38 ± 0.27	-0.39 ± 0.05	4.36 ± 1.52	-8.56	<0.001	[-0.49; -0.30]	-1.75
N13 (vr)	22	17.58 ± 0.22	-0.61 ± 0.07	6.37 ± 1.11	-8.89	<0.001	[-0.75; -0.47]	-1.81
N13 (CCA)	24	17.58 ± 0.25	-0.16 ± 0.02	6.76 ± 1.89	-9.09	<0.001	[-0.20; -0.13]	-1.86
N20 (CCA)	24	23.71 ± 0.24	-0.58 ± 0.06	42.14 ± 15.78	-9.92	<0.001	[-0.70; -0.46]	-2.02
Sensory tibial nerve stimulation (foot-sensory)								
		First toe (toe1)						
N8	20	15.46 ± 0.28	-0.11 ± 0.02	4.05 ± 0.82	-6.33	<0.001	[-0.14; -0.07]	-1.29
N22 (tr)	24	31.21 ± 0.60	-0.17 ± 0.03	2.39 ± 0.69	-6.63	<0.001	[-0.23; -0.12]	-1.35
N22 (vr)	24	31.25 ± 0.60	-0.10 ± 0.02	1.72 ± 0.26	-4.51	<0.001	[-0.14; -0.05]	-0.92
N22 (CCA)	22	31.38 ± 0.52	-0.10 ± 0.01	3.61 ± 0.60	-7.03	<0.001	[-0.13; -0.07]	-1.44
P40 (CCA)	24	49.83 ± 0.71	0.53 ± 0.07	26.84 ± 10.81	7.13	<0.001	[0.38; 0.68]	1.46
		Second toe (toe2)						
N8	20	15.71 ± 0.29	-0.10 ± 0.02	5.49 ± 1.99	-6.32	<0.001	[-0.13; -0.07]	-1.29
N22 (tr)	23	31.25 ± 0.58	-0.21 ± 0.04	2.15 ± 0.32	-5.78	<0.001	[-0.28; -0.13]	-1.18
N22 (vr)	23	31.04 ± 0.62	-0.08 ± 0.02	2.81 ± 0.73	-3.13	0.004	[-0.13; -0.03]	-0.64
N22 (CCA)	23	31.38 ± 0.49	-0.10 ± 0.01	4.20 ± 0.61	-8.64	<0.001	[-0.13; -0.08]	-1.76
P40 (CCA)	23	50.42 ± 0.75	0.62 ± 0.08	26.84 ± 5.50	7.43	<0.001	[0.44; 0.79]	1.52
		First and second toe (toes1&2)						
N8	19	15.33 ± 0.28	-0.19 ± 0.03	9.29 ± 2.92	-6.95	<0.001	[-0.25; -0.13]	-1.42
N22 (tr)	23	31.21 ± 0.60	-0.22 ± 0.02	3.87 ± 0.76	-9.38	<0.001	[-0.26; -0.17]	-1.91
N22 (vr)	23	31.00 ± 0.56	-0.18 ± 0.03	3.40 ± 0.72	-5.27	<0.001	[-0.25; -0.11]	-1.08
N22 (CCA)	23	31.38 ± 0.48	-0.18 ± 0.02	7.59 ± 1.72	-8.44	<0.001	[-0.22; -0.14]	-1.72
P40 (CCA)	23	49.25 ± 0.73	0.81 ± 0.10	26.72 ± 5.66	8.42	<0.001	[0.61; 1.01]	1.72

When we statistically compared amplitude and latency between mixed nerve stimulation and double-digit sensory nerve stimulation we observed that double-digit stimulation (fingers/toes1&2) occurred later and was smaller in amplitude in the spinal cord (Figure 4), a pattern that consistently held also for peripheral and cortical levels (Table 3).

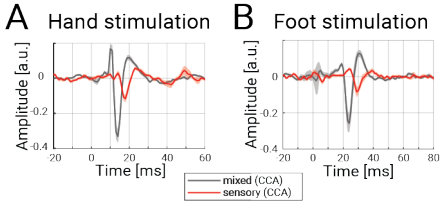

Figure 4. Spinal SEP to mixed nerve and sensory nerve stimulation. *Depicted is the grand average over all participants of Experiment 2 (N=24) in* ***(A)*** *the cervical spinal cord to hand-mixed or fingers1&2 stimulation and* ***(B)***

the lumbar spinal cord to foot-mixed or toes1&2 stimulation. All traces were obtained after CCA and the shaded error-bands reflect the standard error of the mean (note that the increased error-band around 0 ms in the lumbar data reflects remaining stimulus artifacts due to imperfect interpolation).

Potential peaks following double finger stimulation (fingers1&2) occurred 3.91 ms (peripheral), 4.30 ms (spinal), and 3.90 ms (cortical) later than those following hand-mixed stimulation and were 76% (peripheral), 66% (spinal), and 59% (cortical) smaller in amplitude. Potentials following double toe stimulation (toes1&2) occurred 6.05 ms (peripheral), 7.63 ms (spinal), and 8.39 ms (cortical) later compared to mixed nerve stimulation and were 88% (peripheral), 63% (spinal), and 43% (cortical) smaller in amplitude. Altogether, these results replicate previously reported somatosensory potentials along the somatosensory processing hierarchy to mixed hand and foot nerve stimulation as well as to single or simultaneous finger or toe stimulation and provide statistics over the whole sample.

Table 3. *Paired t-test for the comparisons between hand-mixed and fingers1&2 conditions or foot-mixed and toes1&2 conditions. Tested were the amplitudes and the latencies of the SEP or peripheral NAP. Data come only from Experiment 2 (N=24, vr = ventral reference, tr = thoracic reference, CCA – canonical correlation analysis, SEP = somatosensory evoked potential, NAP = nerve action potential).*

SEP / NAP	tstat	p	95%-CI	Cohen's d
Amplitude: Hand-mixed – fingers1&2				
N6	-6.73	<0.001	[-2.41; -1.28]	-1.37
N13 (tr)	-5.38	<0.001	[-0.65; -0.29]	-1.10
N13 (vr)	-7.42	<0.001	[-1.14; -0.64]	-1.52
N13 (CCA)	-9.56	<0.001	[-0.27; -0.17]	-1.95
N20 (CCA)	-10.32	<0.001	[-0.62; -0.41]	-2.11
Latency: Hand-mixed – fingers1&2				
N6	-28.20	<0.001	[-3.94; -3.40]	-5.76
N13 (tr)	-18.10	<0.001	[-4.36; -3.47]	-3.70
N13 (vr)	-18.10	<0.001	[-4.36; -3.47]	-3.70
N13 (CCA)	-21.01	<0.001	[-4.39; -3.61]	-4.29
N20 (CCA)	-32.88	<0.001	[-4.16; -3.67]	-6.71
Amplitude: Foot-mixed – toes1&2				
N8	-5.35	0.001	[-1.09; -0.48]	-1.09
N22 (tr)	-5.50	<0.001	[-0.49; -0.22]	-1.12
N22 (vr)	-5.08	<0.001	[-0.46; -0.19]	-1.04
N22 (CCA)	-7.18	<0.001	[-0.38; -0.21]	-1.47
P40 (CCA)	4.00	0.001	[0.17; 0.55]	0.82
Latency: Foot-mixed – toes1&2				
N8	-24.46	<0.001	[-6.24; -5.26]	-4.99
N22 (tr)	-18.86	<0.001	[-7.86; -6.31]	-3.85
N22 (vr)	-18.86	<0.001	[-7.86; -6.31]	-3.85
N22 (CCA)	-20.82	<0.001	[-7.83; -6.42]	-4.25
P40 (CCA)	-18.56	<0.001	[-9.26; -7.40]	-3.79

Experiments 1 and 2: Robustness of cervical and lumbar spinal SEPs

After i) replicating the recording of the classical spinal SEPs (N13 and N22) and embedding them in the somatosensory processing hierarchy, ii) characterizing their temporal and spatial layout, iii) demonstrating the possibility to obtain them on the single-trial level and iv) extending these results

389 towards purely sensory nerve stimulation, we next aimed at establishing the robustness of the
390 spinal N13 and N22 components of the SEP. Towards this end, we i) investigated how many trials
391 are needed to obtain peak amplitudes significantly different from zero at the single-participant
392 level and ii) determined the joint minimal number of trials and participants needed for a significant
393 effect at the group-level using resampling approaches. These analyses were performed both for
394 SEPs obtained from anatomically-defined target channels and for SEPs obtained via CCA in order
395 to assess whether the multi-channel recording and ensuing spatial filtering approach we employed
396 here might enhance robustness. Since SEPs to mixed nerve (Experiment 1) and sensory nerve
397 stimulation (Experiment 2) differ in their SNR, we performed these analyses for both experiments.

398 Figure 5 displays the results of these analyses in two ways: the left panels show the probability of
399 obtaining a significant SEP at the level of individual participants as a function of trial number
400 whereas the right panels show the probability of obtaining a significant group-level effect for a
401 given combination of trials and participants, i.e., they cater for different research goals. The figure
402 is furthermore split up into results from anatomically-defined target channels (upper rows) vs
403 results obtained via CCA. One effect that is immediately visible – and not too surprising given the
404 different number of activated nerve fibers – is that no matter which outcome is considered, there
405 is a clear order in the level of robustness across the different stimulation conditions, with mixed
406 nerve stimulation giving more robust results than sensory nerve double-stimulation, which in turn
407 leads to more robust potentials than sensory nerve single-stimulation. Thus, whereas in the mixed
408 nerve condition with one target channel, one is almost guaranteed to obtain a significant group-
409 level effect with e.g., ~10 participants and ~200 trials (Figure 3A-B), many more trials and / or
410 participants would be required in the latter conditions to obtain a significant effect and the
411 necessary number can be obtained from the relevant curve or heatmap provided here (Figure 3C-
412 H). This is not meant to dispute that there is clear inter-individual variability in responses (cf.
413 participant #1 and participant #13 in the hand-mixed condition, where approximately 100 vs 1000
414 trials were necessary to obtain a significant result in a majority of repetitions), but in general the
415 mixed nerve conditions allow observing a significant result in the majority of participants with
416 only 200 trials, far from the numbers needed for sensory nerve stimulation.

417 Another effect that is clearly visible from Figure 5 is the beneficial effect of our CCA approach on
418 the robustness of spinal SEPs. In contrast to employing an anatomically-defined target channel,
419 employing CCA required smaller numbers of trials to obtain significant results for each participant
420 in a consistent manner. While this is already visible both at the individual-participant and group-
421 level in the mixed nerve conditions (Figure 5A-B), it becomes even more apparent in the more
422 SNR-limited sensory nerve conditions (Figure 5C-H). For instance, for single-digit stimulation of
423 the index finger and an anatomically-defined target channel (Figure 5E), the use of 24 participants
424 and 1000 trials was necessary to obtain a significant group-averaged result with a probability of
425 0.8. In contrast, with the use of CCA, either the same number of participants with ~200 trials or
426 15 participants with ~500 trials were already enough to achieve similar results.

427

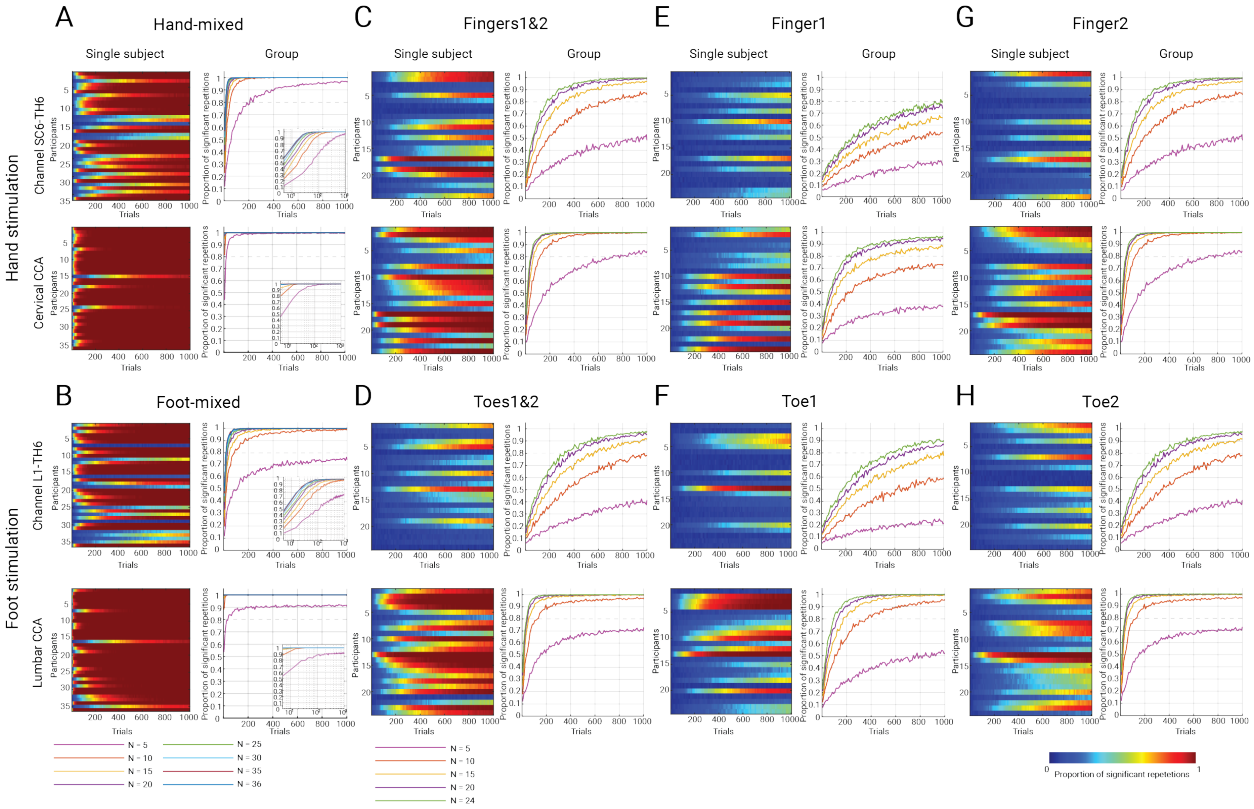

Figure 5. Robustness of spinal cord SEPs. *Robustness is assessed via resampling approaches both at the level of individual participants (heatmaps) and at the group level (line plots). The heatmaps of each subfigure display the proportion of significant repetitions for each participant as a function of trial number (horizontal axis: number resampled of trials, vertical axis: participants) for the anatomically-defined target channel (top left panel) and for CCA (bottom left panel). The line plots of each subfigure display the probability of obtaining a significant SEP as a function of trial number and sample size (in the Monte Carlo simulations) for the anatomically-defined target channel (top right panel) and for CCA (bottom right panel); the insets for the mixed nerve stimulation use a logarithmic scale to provide more details. The different panels display the different conditions: hand-mixed **(A)** and foot-mixed **(B)** in 36 participants (Experiment 1); hand-sensory in 24 participants (Experiment 2) in the simultaneous finger stimulation condition **(C)**, and the single finger stimulation conditions **(E and G)**; foot-sensory stimulation in 24 participants (Experiment 2) in the simultaneous toe stimulation condition **(D)**, and the single toe stimulation conditions **(F** and **H)**. In order to clearly convey the pattern of results, only up to 1000 trials are displayed.*

Experiment 2: Effects of stimulation condition are shared across the somatosensory hierarchy

We next turned to investigating whether response properties are shared across the somatosensory hierarchy. More specifically, we were interested in whether changes in response amplitude across the somatosensory hierarchy would be fully explained by the stimulation condition or whether additional predictive links between the hierarchical levels would be detectable in our data. Towards this aim, we compared the four different conditions presented in Experiment 2, which differ in the number and type of stimulated nerve fibers, with the mixed-condition activating a much broader extent of fibers than the sensory condition, which is consequently also reflected in the lower potential amplitudes for sensory conditions. Taking advantage of the possibility to extract single-trial cortical and spinal SEP amplitudes via CCA (as demonstrated above for the

data from Experiment 1), we examined the covariance of single-trial amplitudes of the neural responses along the somatosensory processing hierarchy with linear-mixed-effects (LME) models: peripheral NAP amplitudes were used to predict spinal SEP amplitudes and spinal SEP amplitudes were used to predict cortical SEP amplitudes, with the hypothesis of a positive relationship between potentials of the same direction and a negative relationship between potentials of opposite direction. In order to understand the contribution of the stimulation condition, LME models were fitted stepwise to the single-trial amplitudes, also including stimulation condition as a predictor (with the levels mixed nerve, finger1/toe1, finger2/toe2, fingers1&2/toes1&2). Detailed results are provided in the Supplementary Material section IV, with the two main observations being that i) response properties are shared across the somatosensory hierarchy and ii) most of their variance is explained by the stimulation condition. In other words, the effects of different stimulation types propagate through the somatosensory processing hierarchy, jointly affecting the amplitudes of peripheral NAPs, spinal cord responses, and initial cortical potentials in the primary somatosensory cortex (for both hand and foot stimulation). Interestingly however, in the foot stimulation condition, additional condition-independent effects of spinal amplitudes on cortical amplitudes were observed, providing a trial-by-trial spino-cortical link.

Experiment 2: Attenuation effect on SEP amplitudes

Finally, we aimed to study a well-known phenomenon in somatosensory processing, namely attenuation effects (also referred to as interaction or gating effects). These are observed, for example, when electrically stimulating two adjacent fingers, where the cortical SEP following simultaneous stimulation of both fingers is attenuated compared to the sum of SEPs to single finger stimulation due to integrative processes. While this effect is well studied at the cortical level and has been hypothesized to occur subcortically already (Biermann et al., 1998; Gandevia et al., 1983; Hoechstetter et al., 2001; Hsieh et al., 1995; Ishibashi et al., 2000; Ruben et al., 2006), there is so far only anecdotal evidence for such attenuation occurring already at the spinal level (El-Negamy & Sedgwick, 1978; Gandevia et al., 1983). Therefore, a major aim of Experiment 2 was to investigate this attenuation effect on SEP amplitudes at peripheral, spinal and cortical levels. While we expected that peripheral NAPs should faithfully reflect the given stimulation (considering that there are no synaptic relays yet) and thus not show attenuation effects, we did expect to observe such effects not only at the cortical level (where it has previously been reported), but also at the spinal level (due to the enhanced sensitivity made possible by our multi-channel spatial filtering approach).

To test these hypotheses, we obtained CCA-extracted amplitudes of cortical and spinal SEP as well as peripheral NAP amplitudes to single-digit stimulation and simultaneous digit stimulation and assessed the attenuation effect via interaction-ratios (IR). The IR is a measure that quantifies (in percent) the amplitude reduction of the simultaneous digit stimulation compared to the arithmetic sum of the single-digit stimulations for each participant. After finger stimulation, significant attenuation effects were observed for the cortical N20 ($mean\ IR = 22.21\%$, $t(23) = 9.03$, $p < 0.001$, $95\%\text{-}CI = [17.12\%; 27.30\%]$, $d = 1.84$) and the cervical N13 ($mean\ IR = 20.25\%$, $t(20) = 5.16$, $p < 0.001$, $95\%\text{-}CI = [12.06\%; 28.43\%]$, $d = 1.13$), but not for the peripheral N6 ($mean\ IR = -1.83\%$, $t(22) = -0.60$, $p = 0.56$, $95\%\text{-}CI = [-0.17\%; 4.50\%]$, $d = 0.13$). We observed a similar

pattern of results for toe stimulation, where significant attenuation effects were observed for the cortical P40 (*mean IR* = 26.07%, *t(22)* = 6.56, $p < 0.001$, *95%-CI* = [17.83%; 34.32%], $d = 1.37$), for the lumbar N22 (*mean IR* = 10.25%, *t(21)* = 2.51, $p < 0.020$, *95%-CI* = [1.76%; 18.75%], $d = 0.54$), but not for the peripheral N8 (*mean IR* = 6.99%, *t(18)* = 0.84, $p = 0.432$, *95%-CI* = [−11.28%; 25.27%], $d = 0.19$). Figure 6 displays the results as grand average time traces and IR at the spinal, cortical and peripheral levels. Taken together, our results indicate that robust attenuation effects in somatosensation are not an exclusively cortical phenomenon, but already occur at the level of the spinal cord.

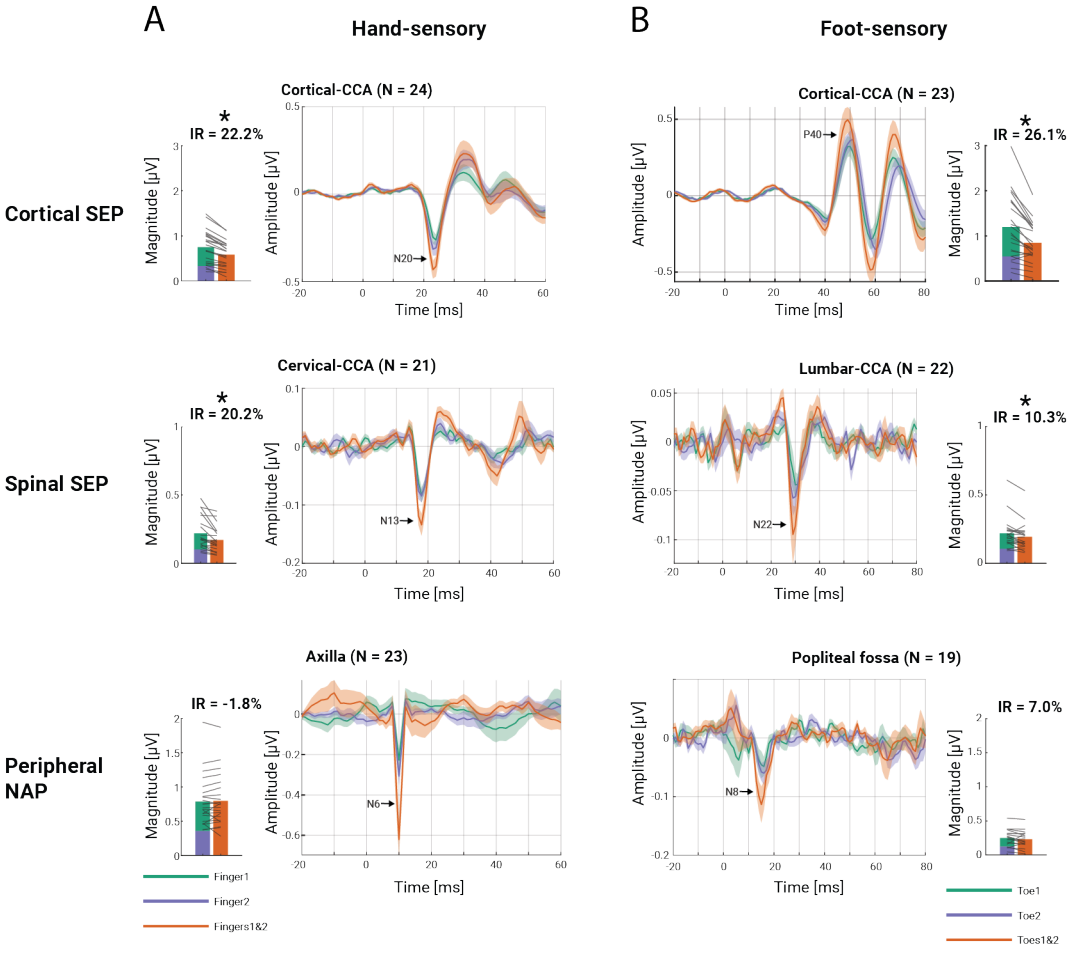

Figure 6. Attenuation effects at cortical, spinal, and peripheral levels. (A) *Potentials following finger stimulation (from top to bottom): cortical N20 amplitudes, spinal N13 amplitudes, peripheral N6 amplitudes.* ***(B)*** *Potentials following toe stimulation (from top to bottom): cortical P40 amplitudes, lumbar N22 amplitudes, peripheral N8 amplitudes. The traces in the middle columns display the grand-average response over participants to single-digit stimulation (green and blue traces) and double-digit stimulation (red trace), with the error-band displaying the standard error of the mean. The bar plots in the outer columns display the group average of summed potential amplitudes to single-digit stimulation (green and blue bars) and double-digit stimulation (red bar), with grey lines depicting single-participant data. Please note that i) slightly different numbers of participants entered the analyses at the different levels (only those with identifiable and unbiased potentials), ii) the latency terminology used here is based on mixed nerve latencies (sensory nerve potentials occur later), and iii) the scaling of the vertical axes is different between the bar-plots and the traces (since the bar plots depict magnitude data and are furthermore based on extracted potential amplitudes at latencies where individual participants had the strongest amplitude).*

Discussion

Here, we report the development of a multi-channel electrophysiology approach to non-invasively record spinal cord potentials with high precision and incorporate these responses within a comprehensive picture of processing along the somatosensory hierarchy (from peripheral nerves to somatosensory cortex). For all aspects addressed in the two separate experiments, we employ stimulation of both the upper and lower limb and accordingly report responses in the cervical and lumbar spinal cord, respectively. We compare responses to stimulation types with different signal-to-noise levels (i.e., all fibers of a nerve versus only part of the sensory nerve fibers), provide a spatiotemporal characterization of spinal responses (i.e., assessing early and late potentials, frequency content and spatial distribution), and embed these responses within the different somatosensory processing levels. Using adequately powered (and pre-registered) sample sizes, we report SEPs to mixed and sensory nerve stimulation at single, anatomically-defined target channels. Going beyond this, we show that analyzing SEPs in a multivariate way, that is, reweighting the multi-channel signal on a participant-by-participant basis using canonical correlation analysis (CCA), results in an enhanced sensitivity and – even more important – allows for single-trial estimation of spinal cord SEPs. Finally, we apply the developed approach to a neuroscientific question, namely the investigation of integration effects along the somatosensory hierarchy, which we observe to not only occur at the cortical, but already at the spinal level. In order to allow others to seamlessly build upon our results, we make data as well as code openly available and also carry out replication and robustness analyses, thus providing a status quo of what is currently feasible with electrospinography.

Characterizing spinal cord somatosensory evoked potentials

Spinal cord SEPs have been studied intensively in the last century, starting with their discovery in humans in an invasive study (Magladery et al., 1951; following up on the first recordings of cord-dorsum potentials in cats by Gasser & Graham, 1933) and followed about 15 years later with the first non-invasive recordings of spinal SEPs (Cracco, 1972, 1973; Jones, 1977; Liberson et al., 1966; Matthews et al., 1974). During the development of the field, a large number of studies focused on developing procedures that might help with diagnostic processes (for review, see Cruccu et al., 2008; Mauguiere, 1996; Mauguière et al., 1999), e.g., investigating the latency of spinal SEP components since this has direct clinical relevance for the measurement of peripheral and central nerve conduction velocities. Apart from this clinical focus, an important question that was affirmatively answered was whether the canonical spinal SEPs (cervical N13 and lumbar N22) have a post-synaptic origin (for review see Mauguière, 2000; Yamada, 2000). Here, we aimed to replicate and build upon findings from this large body of literature (>150 publications in healthy humans) on non-invasive spinal cord SEPs in healthy humans.

First, we simultaneously recorded peripheral, spinal, brainstem and cortical responses to electrical stimulation of a mixed nerve in the upper- and lower-limbs and depicted responses of the temporal progression of the signal along the somatosensory processing hierarchy. In contrast to previous studies, we depicted grand-average group-level responses and reported associated statistics for each potential (including effect sizes to help in the planning of future studies); the main results of these analyses were then replicated in an independent sample of participants. *Second*, we compared spinal SEPs following sensory nerve stimulation (at the digits) to SEPs following mixed nerve

stimulation (at wrist and ankle) and observed reduced peak amplitudes and increased latencies (4.3 ms and 7.6 ms at the cervical and lumbar level), likely due to the lower number of fibers being activated and the additional distance of nerve impulses to travel, respectively. Reassuringly though, even with single-digit stimulation, we observed mostly large effect sizes for spinal SEPs, hinting at the potential of ESG to also record responses to ecologically more valid stimulation (e.g., in the domain of nociception), that is expected to have an even lower SNR. *Third*, we made use of our multi-channel setup to investigate the spatial distribution along the neck and trunk of the main negative deflection of the tri-phasic mixed nerve SEPs: both presented as radial dipoles with a slight shift compared to the expected center (slightly above the spinous process of vertebra C6 for the N13 and slightly below the spinous process of vertebra L1 for the N22). Their sagittal center was over the cord, which also speaks against a myogenic origin as trunk muscle responses tend to present with a more lateralized distribution (Jiang et al., 2021; see also El-Negamy & Sedgwick, 1978 who ruled out a myogenic origin pharmacologically). To the best of our knowledge, such a spatial characterization of spinal SEPs has not been carried out so far (see Desmedt & Huy, 1984 for a limited spatial window on cervical potentials). Even modern MSG-studies are currently limited to cervical or lumbar windows when investigating spatial properties of spinal somatosensory evoked fields (Akaza et al., 2021; Ushio et al., 2019), whereas our approach allows for a more holistic view. Obviously, the here presented non-invasive electrophysiological data do not allow for conclusions regarding the exact origin of these potentials within the spinal cord, but previous animal work suggests that these potentials are generated by interneurons in the deep dorsal horn (e.g., Beall et al., 1977; Willis et al., 1973; for review, see Shimoji, 1995), likely as part of the post-synaptic dorsal column pathway, which is a prominent source of tactile input to the dorsal column nuclei (Giesler et al., 1984; Turecek et al., 2022; for review, see Brown, 1981).

Two methodological aspects are also worth mentioning. *First*, our data demonstrate that the location of the ESG reference plays a role. Prevertebrally-located non-cephalic references (over the glottis for cervical recordings and above the umbilicus for lumbar recordings in our case) have been reported to optimally capture the dipole of the spinal SEPs and thereby improve their extraction (Desmedt & Cheron, 1981b, 1983a; for review see Desmedt, 1985). Our data are in line with these reports for the cervical potentials, but not for the lumbar ones where no improvement was noticed (but also no deterioration). This could be due to the longer distance between pre- and postvertebral channels at the lumbar level, which can be overcome by using a deep oesophagal electrode (Desmedt & Cheron, 1983a), an approach we did not pursue here. *Second*, it was recognized early on (e.g., Cracco, 1973) that the electrical field produced by the heart activity dominates the recorded ESG signal. Previous studies have either addressed this issue by averaging a high number of trials (with suggested trial numbers between 1000-2000 stimuli; Cruccu et al., 2008) or by delivering stimuli time-locked to the cardiac cycle (for example, Cracco, 1973). Here, we took a different approach and removed the cardiac-artifact with a template-based subtraction-approach that we adopted from the simultaneous EEG-fMRI literature (Niazy et al., 2005; see Chander et al., 2022 for another subtraction-based approach for denoising ESG data). Compared to the previous approaches, this directly addresses the artefact that typically obscures spinal SEPs and therefore allows for i) lower trial numbers (making new types of paradigms feasible), ii) application of stimuli with frequencies higher than the heart rate (shortening experimental duration), and iii) stimulation spaced across the cardiac cycle (allowing to study somatosensory-cardiac interactions).

Spatial filtering improves extraction of spinal potentials on a single-trial level

Traditionally, the analysis of lumbar and cervical potentials is based on averaging a high number of trials of single-channel data, with most studies using single or very few numbers of spinal electrodes. Even when studies used a larger number of spinal electrodes to assess spatial properties, most attached them in a rostrocaudal manner centrally along the spine and investigated the single channels separately (Cracco, 1973; Emerson et al., 1984; Yamada et al., 1982). Methodological advances in EEG data acquisition and analysis in the last three decades now allow for a better separation of signal from noise and use high-density electrode montages for construction of spatial maps, in which the data of the whole set of EEG electrodes can be treated as a multivariate signal (Lopes da Silva, 2013; Michel & Murray, 2012).

Our high-density spinal electrode montage thus allowed for the application of methods that combine the information from many channels via spatial filters. Specifically, we used a CCA-based approach that has been applied in several EEG studies for extraction of early cortical SEPs (Fedele et al., 2013; Stephani et al., 2020, 2021, 2022; Waterstraat et al., 2015) and returns spatial filters with weights for the different channels based on their contribution to the evoked potential. In the present study, we show that spinal SEP extraction is markedly improved when employing such a multi-channel spatial filtering approach. We believe that this approach will be especially beneficial for analyzing evoked responses from the spinal cord for two reasons. First, the ESG signal is particularly affected by physiological noise sources (e.g., from cardiac and myogenic sources; Cracco et al., 1973), leading to a low SNR context where single-trial amplitudes are hidden in background noise. Second, there are substantial inter-individual differences in the relative location of spinal segments relative to spinal vertebrae (Cadotte et al., 2015; Reimann & Anson, 1944). Since the spinal vertebrae are used as anatomical landmarks for the placement of ESG electrodes, a spatial filter that compensates for such inter-individual differences can be beneficial for analyses at the group-level, but also for recovering signals in individual participants, where an electrode placed on a specific anatomical landmark might not capture the spatial peak of the response.

By improving the SNR of ESG data, our spatial filtering approach allows not only for extracting more robust spinal SEPs with a reduced number of trials, but also for studying the variability in spinal SEP amplitudes at a single-trial level. This will be of benefit for domains where massive trial-averaging is not possible (e.g., in pain research) or for paradigms where only a few or even single trials are of interest (e.g., in omission designs). Another use case for single-trial analyses is to assess how response amplitudes co-fluctuate across different processing levels (i.e., from periphery to spinal cord to cortex), which we tested here. We observed that the effects of different stimulation conditions (i.e., single-digit, double-digit, and mixed nerve) corresponded to shared variance across the early somatosensory processing hierarchy, encompassing peripheral NAPs, spinal SEPs, and early cortical SEPs. Presumably, this covariance reflected the number of stimulated nerve fibers that can be expected to have varied between stimulation conditions (i.e., mixed nerve stimulation activates more nerve fibers than double- and single-digit stimulation). However, additional condition-independent variations in the foot stimulation might be worth further investigation: here spinal response amplitudes predicted early somatosensory cortex response amplitudes, providing a spino-cortical link on the single-trial level.

Later spinal SEP components

Having focused on the canonical early spinal SEPs (N13 and N22), we also aimed at investigating whether late potentials could be detected in the ESG traces. Using cluster-based permutation tests on the mixed nerve data from Experiment 1, we observed significant later-occurring positive SEP components that directly followed the cervical N13 or the lumbar N22: these were observed from 17-35 ms and 28-35 ms for the cervical and lumbar recordings, respectively and were both replicated when using mixed nerve data from an independent sample of participants in Experiment 2. Similar late potentials have already been descriptively mentioned as part of a tri-phasic wave in some of the earliest invasive epidural / intrathecal and non-invasive surface recordings following median and tibial nerve stimulation (Cracco, 1972, 1973; Ertekin, 1976; Shimoji et al., 1972), but here we provide firm statistical evidence for their existence at the group-level.

With respect to the origin of these late potentials, a myogenic source has been ruled out by experiments that employed using muscle relaxants in epidural recordings (Shimoji et al., 1972). It might be possible that the cervically observed late potential could – to a certain degree – also reflect a contribution from late top-down brainstem potentials (Hsieh et al., 1995), also considering its slightly rostral spatial distribution and prolonged duration compared to the late lumbar potential. In general, we believe though that the non-cephalic reference used in our spinal montage and the fact that the positive late components are present at lumbar as well as cervical spinal levels clearly speaks against a leaking far-field potential from sources in the brain and thus points towards a local spinal origin. The exact neurophysiological mechanism remains to be clarified, but there are indications for such late positive components to represent primary afferent depolarization (Shimoji, 1995). In future studies, a local spinal origin of these late potentials could be even more firmly established by using spatially more extended dense electrode grids.

We further observed an ultra-late negative lumbar potential following tibial nerve stimulation between 126-132 ms. To our knowledge, no spinal SEPs have hitherto been reported at such latencies, even though there are hints for the existence of such responses in early neuromagnetic neck recordings (Mizutani & Kuriki, 1986). We were however not able to replicate this ultra-late potential in Experiment 2, which could either be due to this being a false-positive result or to the reduced sample size and the reduced inter-stimulus interval in Experiment 2, thus awaiting further studies for clarification. Taken together, the possibility to detect late spinal potentials opens the door for investigating local processing within the spinal cord that goes beyond a simple relay of information (Abraira et al., 2017) as well as supra-spinal modulatory influences on innocuous and noxious stimulus processing in the dorsal horn (Liu et al., 2018).

Attenuation effects are present at spinal and cortical but not at peripheral levels

One fundamental question in research on sensory processing is at which levels of the processing hierarchy information from the receptors is integrated. Here, we assessed this question in somatosensation by testing for integrative processes at peripheral, spinal and cortical levels. We used the previously developed CCA approach (Experiment 1) to extract SEP amplitudes to single-digit and double-digit stimulation (Experiment 2) and quantified the attenuation effect – which reflects a reduced response to double-digit stimulation compared to the summed-up responses to

single-digit stimulation – as a measure of integration. The sensory nerve stimulation data we obtained in Experiment 2 show that significant integration effects to double finger stimulation and to double toe stimulation are present with medium to large effect sizes in the central nervous system – both at cortical and at cervical and lumbar spinal levels – but not in the peripheral nervous system, i.e., only evident after at least one synaptic relay. Interestingly, while the attenuation is significant at both cortical and spinal levels, the effect size is much larger cortically. The cortical findings are in line with several previous studies (Biermann et al., 1998; Gandevia et al., 1983; Hoechstetter et al., 2001; Hsieh et al., 1995; Huttunen et al., 1992; Ishibashi et al., 2000; Okajima et al., 1991; Ruben et al., 2006; Severens et al., 2010; Tanosaki et al., 2002), but the robust spinal results (observed for upper and lower limb stimulation) go beyond the previous literature, where only anecdotal evidence of such effects existed at the cervical level (El-Negamy & Sedgwick, 1978; Gandevia et al., 1983). While the simultaneous recording and assessment of integration effects at peripheral, spinal and cortical levels is a first to our knowledge, a progression of increasingly stronger integration effects along the neural hierarchy – as present in our data – has also been reported from brainstem to cortex based on invasive recordings (Hsieh et al., 1995), where this was linked to increasing receptive field size along the neural hierarchy.

Two mechanisms have been discussed to underlie integration effects as observed here: occlusion (Gandevia et al., 1983) and active lateral inhibition (Gandevia et al., 1983; Severens et al., 2010; Tanosaki et al., 2002). Occlusion occurs in neurons that respond to the stimulation of both digits, which might in turn have a reduced response to simultaneous stimulation, reflected in a reduced SEP amplitude, when comparing it to the summed SEP amplitude of single-digit stimulation. Active lateral inhibition can occur in groups of neurons that are spatially close to each other and can therefore inhibit each other when stimulated simultaneously. Either mechanism could be at work in the spinal cord, considering for example the integrative nature of many deep dorsal horn interneurons (Abraira et al., 2017) and the receptive-field organization of wide dynamic range neurons (Le Bars & Cadden, 2008). Targeted experimental designs to dissociate these two mechanisms – as already employed at the cortical level (Severens et al., 2010) – would help to shed more light on the underlying processes at the spinal level.

Insights for planning future electrospinography experiments

The literature on non-invasive electrospinographic recordings from the human spinal cord spans more than 50 years (Liberson et al., 1966) and contains important normative data for SEP latencies for example (Synek, 1986a, 1986b; Tsuji et al., 1984). However, since the issue of underpowered studies in neuroscience rose to prominence (Button et al., 2013), only very few spinal cord SEP studies have been published (Boehme et al., 2019; Chander et al., 2022; Di Pietro et al., 2021; Fabbrini et al., 2022; Rocchi et al., 2018) and there is thus a lack of data that would help with planning well-powered and reproducible experiments in this domain. Here we set out to fill this gap in two ways.

First, we followed the general recommendation of using 1000-2000 stimuli in order to have an adequate signal-to-noise ratio for robust spinal SEP extraction (Cruccu et al., 2008) and then reported group-level confidence intervals and effect sizes for all investigated potentials in both studies, hoping that this might serve as an initial guide for sample-size estimations of future experiments with similar settings. Reassuringly, the obtained effect sizes were highly similar across both experiments and consistently in the large range (with the exception of brainstem

potentials and responses to single-digit stimulation). Such large number of stimuli might however not be feasible for all types of experiments (e.g., when several different conditions or long inter-trial-intervals are necessary). In a second approach based on resampling procedures, we therefore i) estimated the minimal number of stimuli necessary to obtain a significant result with a certain probability at the individual-participant-level and ii) jointly estimated the minimal number of stimuli and participants to obtain a significant result with a certain probability at the group-level. Simulating experiments this way (see also Boudewyn et al., 2018) allows for giving specific recommendations, such as that for mixed nerve stimulation acquiring ~200 trials in ~10 participants almost guarantees a significant group-level effect, whereas for single-digit sensory nerve stimulation ~1000 trials in ~24 participants are necessary to obtain a significant group-level effect with a probability of 0.8 when using single-electrode data (though other factors such as general data quality, participant population, experimental paradigm etc. should obviously be considered). One other insight gained from these simulations is the clear advantage offered by multi-channel spinal cord recordings with subsequent spatial filtering approaches (CCA in our case). These present with enhanced robustness, as their use leads to a strong reduction in the number of trials or participants necessary to obtain significant spinal SEPs compared to the single-electrode simulations, especially so in low SNR situations such as single-digit stimulation.

Limitations

There are several limitations of our approach that are worth mentioning. A first possible limitation is the positioning of the participants (who were lying on their back, i.e., on the electrodes), which could possibly lead to a higher noise level in the ESG data due to electrode movements. There are several alternative positions (e.g., participants lying on the side or in a prone position, sitting in a chair without backrest, etc.), but after pilot experiments, we decided to record data in supine position, as this seemed to offer the most comfort over the course of the experiment without degrading data quality (e.g., due to tonic muscle activity).

Second, while other ESG studies have also used our choice of reference position for the recording of cervical and lumbar SEPs (Berić, 1988; Delbeke et al., 1978; M. R. Dimitrijevic et al., 1978, 1980; Gilmore et al., 1985; Lastimosa et al., 1982; Maccabee et al., 1983; McKay & Galloway, 1979; Ratto et al., 1983), the choice of reference position is always a compromise. For spinal recordings a non-cephalic reference as used here is generally suggested, but studies often use different references for cervical and lumbar recordings, such as the acromion for cervical or the pelvic bone for lumbar recordings. We wanted to use a reference position that is i) not lateralized, ii) ideal for both cervical and lumbar recordings and iii) positioned on a bone (not on muscle) and thus selected the spinous process of the 6th thoracic vertebra after running several pilot recordings with different reference positions.

Third, we had hoped to reliably record brainstem SEPs arising from the cuneate nucleus (N14) (Suzuki & Mayanagi, 1984) and gracile nucleus (N30) (Tinazzi et al., 1996), as these are targets of the post-synaptic dorsal column pathways, i.e., direct recipients of output from the spinal cord. Brainstem SEPs are typically recorded as far-field potentials between a non-cephalic reference and Fz (Mauguière et al., 1999), but can be recorded between the brainstem and a frontal channel as well (Restuccia et al., 1995; Tinazzi et al., 1995, 1996). Despite using optimal signal extraction leads here, observing brainstem potentials was not possible in all conditions, mainly due to the

775 limited SNR of SEPs to digit stimulation, where most participants did not show brainstem
776 potentials.

777 Fourth, we intended to stimulate mixed and sensory parts of the same nerve. However, when
778 stimulating the fingers or toes, it is not possible to clearly differentiate which nerve is stimulated,
779 since there is an individual variability in the spatial distribution of the dermatomes (Dykest &
780 Terzis, 1981; Lee et al., 2008). Therefore, it is important to keep in mind when interpreting our
781 results that during stimulation of the index and middle finger, sensory fibers of the median as well
782 as the ulnar and radial nerve might be stimulated (lower limb: sensory fibers of the superficial and
783 deep peroneal nerves).

784 Finally, it is important to point out that this study served to introduce a novel methodological
785 approach (multi-channel spinal cord recordings with ensuing spatial filtering that allows for single-
786 trial analysis across the neural hierarchy) and is thus mostly focused on the detection of spinal cord
787 SEPs to *carefully controlled* somatosensory stimulation that gives rise to a *strongly synchronized*
788 signal of high amplitude. One might therefore question the ecological validity of the type of
789 stimulation employed here and consequently doubt whether this method will also perform well
790 under more naturalistic stimulation conditions, such as innocuous or noxious mechanical or
791 thermal stimulation. We believe, however, that the combination of methodological improvements
792 introduced here should also be helpful in such low-SNR scenarios, as e.g., already demonstrated
793 in the case of single-digit sensory nerve stimulation.

794

795 ***Outlook and conclusion***

796 In conclusion, we aimed to establish an approach for the non-invasive recording of spinal cord
797 responses that is more easily accessible and widely available than current alternatives such as
798 spinal cord fMRI or MSG. It allows for a direct recording of electrophysiological responses with
799 high temporal precision (allowing to investigate different response components, i.e., early and late
800 potentials), has a high sensitivity due to its multi-channel nature (including single-trial estimates),
801 and is integrated with the recording of afferent and efferent signals (peripheral and supra-spinal
802 responses). We believe that this approach could be extended to other types of natural stimulation
803 (e.g., social touch or pain) and might not only be suitable for investigating purely bottom-up
804 processes, but also their modulation by various factors (Cohen & Starr, 1985; Di Pietro et al.,
805 2021). One might also consider combining our approach with simultaneous fMRI data acquisition
806 – given the latter's high spatial resolution – to harness their individual strengths: here, one might
807 either assess interactions between spinal and supra-spinal levels using simultaneous corticospinal
808 protocols (Finsterbusch et al., 2013) or make use of the increased spatial resolution offered by
809 higher field strengths (Barry et al., 2018) to temporo-spatially resolve functional units within the
810 spinal cord. Taken together, we hope to have provided an approach that allows for a sensitive and
811 direct assessment of spinal cord responses – as well as their input and output signals – and
812 anticipate its use in the context of interrogating the spinal cord's role in the interplay of bottom-up
813 and top-down processes that together give rise to our sensations.

814

815

Materials and Methods

Experiment 1

1.1: Participants.

42 healthy right-handed volunteers participated in this experiment. Two participants were not able to successfully complete the experiment (cigarette craving in one case, bathroom use in another case) and their data were thus discarded. Four participants were excluded due to absent peripheral potentials, leading to a final sample size of 36 participants (18 female; age: 25.5 ± 3.5 years (mean ± SD)). All participants provided written informed consent and the study was approved by the Ethics Committee at the Medical Faculty of the University of Leipzig. Please note that the final sample-size of 36 participants was specified in a pre-registration prior to the start of the study (see section 'Open science') and was chosen in order to detect a medium-sized effect (Cohen's d = 0.5) with a power of 90% (at an alpha-level of 0.05 with one-tailed testing).

1.2: Experimental Design.

The experiment had a repeated-measures design, meaning that each participant underwent all experimental conditions. The experiment consisted of two conditions, named hand-mixed and foot-mixed in the following. In the hand-mixed condition, the left hand of the participant was stimulated with electrical pulses to the median nerve at the wrist. In the foot-mixed condition, the left foot of the participant was stimulated with electrical pulses to the posterior tibial nerve at the ankle. We refer to these conditions as 'mixed', because at the wrist and the ankle, the median and tibial nerve, respectively, are mixed nerves, i.e., contain both sensory and motor nerve fibers. Figure 1A displays the experimental timeline of Experiment 1.

1.3: Electrical stimulation.

The electrical stimulus was a 0.2 ms square-wave pulse delivered by two constant-current stimulators ("DS7A", Digitimer Ltd, Hertfordshire, UK; one stimulator for each nerve) via a bipolar stimulation electrode with 25 mm electrode distance ("reusable bipolar stimulating surface electrode", Spes Medica, Genova, Italy) to the left median or the left posterior tibial nerve, respectively. The stimulation electrodes were placed (with the cathode being proximal) at the palmar side of the wrist (median nerve stimulation) and at the median side of the ankle (posterior tibial nerve stimulation). The stimulation intensity was set to just above the individual motor threshold, which was defined as the intensity at which a participant's thumb or first toe started to twitch (visually determined). All participants perceived the stimulation intensity as a distinct, but not painful, sensation.

1.4: Electrographic recordings.

All electrographic signals were recorded with TMS-suitable Ag/AgCl electrodes ("TMS-compatible multitrodes", Easycap GmbH, Herrsching, Germany). For electroencephalography (EEG), 64 electrodes were arranged on an EEG cap (Easycap GmbH) with standard positions according to the 10-10 system and referenced to the right mastoid (RM). Recorded EEG- channels were: Fp1, Fp2, F3, F4, C3, C4, P3, P4, O1, O2, F7, F8, T7, T8, P7, P8, AFz, FCz, Cz, Pz, FC1, FC2, CP1, CP2, FC5, FC6, CP5, CP6, FT9, FT10, LM (left mastoid), Fz, F1, F2, C1, C2, AF3, AF4, FC3, FC4, CP3, CP4, PO3, PO4, F5, F6, C5, C6, P5, P6, AF7, AF8, FT7, FT8, TP7, TP8, PO7, PO8, FPz, CPz, F9, and F10. An active ground electrode was placed at POz.

For electrospinography (ESG), 39 electrodes were placed on the upper body, with the largest part of the electrodes placed into one cervical and one lumbar electrode patch. These patches were custom-made and consisted of the same fabric used for the EEG cap (kindly provided by Easycap GmbH). ESG data was referenced to an electrode positioned over the spinous process of the 6th thoracic vertebra (TH6) and the following electrodes were located at anatomical positions: electrode SC1 at the 1st cervical vertebra, electrode SC6 at the spinous process of the 6th cervical vertebra, electrode L1 at the spinous process of the 1st lumbar vertebra, and electrode L4 at the spinous process of the 4th lumbar vertebra. An additional 16 electrodes were organized in a grid around each one of the two spinal target electrodes SC6 and L1 (Figure 1). The grid organization, which was developed in pilot experiments, aimed at capturing the spatial distribution of the spinal signal. The midline of this grid was positioned vertically on the spine and consisted of 5 electrodes (the 3rd one being the spinal target electrode) with a vertical inter-electrode distance of 2 cm. Two further vertical lines of 4 electrodes each were placed 1 cm to the right and left of the midline electrodes and another two vertical lines of two electrodes each were placed 5 cm to the right and left of the midline. In addition to these dorsally placed electrodes, there were two ventrally placed electrodes – one supra-glottic (AC) and one supra-umbilical electrode (AL). Such ventral electrodes have been described to be beneficial for SEP extraction in the literature (Desmedt & Cheron, 1981a, 1983a; Desmedt & Huy, 1984; Restuccia et al., 1995). Because the EEG and ESG montage used different references, we added Fz to both montages with channel name "Fz" in the EEG montage and "Fz-TH6" in the ESG montage, as this allows to combine the two montages into one by re-referencing at a later point. In 6 out of the 36 participants (sub-001 to sub-006) Fz-TH6 was missing in the ESG setup due to a technical error. The active ground electrode stabilized the signal via the "driven right leg" principle. It was placed at POz in the EEG montage and in the middle between TH6 and S20 in the ESG montage.

In addition to EEG and ESG, we also recorded several other types of data. First, electroneurographic (ENG) data – i.e., peripheral nerve action potentials (NAPs) – of the median nerve were recorded at the level of the left axilla (over the biceps, reference electrode proximal, distance 3 cm between electrodes) and the left Erb's point (referenced to right Erb's point). Peripheral NAPs of the posterior tibial nerve were recorded from the popliteal fossa (with 5 electrodes: one electrode was placed in the center of the fossa and 4 electrodes around it at a distance of 1 cm; all knee channels were referenced to a 3 cm proximal electrode). Second, electrocardiographic (ECG) data were recorded from an electrode placed at the left lower costal

arch and referenced to a right sub-clavicular electrode. Third, electromyographic (EMG) data were recorded at the hand from the abductor pollicis brevis muscle and at the foot from the flexor hallucis brevis muscle, with the EMG electrode being placed over the muscle belly and the reference electrode being proximal (please note that EMG data are not reported in this manuscript). Fourth, we recorded the participants' respiratory activity (with a respiration belt: "reusable respiratory effort sensor", Spes Medica S.r.l., Genova, Italy; data also not reported here).

We aimed at keeping impedances at all electrodes below 10 kOhm. All electrographic signals were recorded with NeurOne Tesla amplifiers and software (Bittum Corporation, Oulu, Finnland), applying an anti-aliasing filter at 2500 Hz with a lower cutoff at 0.16 Hz and sampled at a rate of 10000 Hz.

1.5: Experimental procedure.

First, the EEG, ESG, ENG, EMG, and ECG electrodes were attached to the participant's skin. Next, the respiration belt was attached at the level of the $9^{th}/10^{th}$ rib. Then participants were asked to lay down on a cushioned bench on their back in a semi-darkened and acoustically shielded EEG-cabin. For participant comfort, the head support of the bench was slightly raised and a cushion roll was placed under their knees. Next, electrical stimulation location and intensity were determined and participants were instructed to look at a fixation cross during the stimulation blocks, which was attached to the ceiling. The experiment started with 5 minutes of resting-state recording (eyes open) followed by eight stimulation blocks, each consisting of 500 stimuli. During one block, stimuli were delivered to one nerve only, i.e., either the median or the posterior tibial nerve (thus, there were four median and four posterior tibial nerve stimulation blocks in total). The stimulation blocks were presented in alternating order and the order was counterbalanced across participants. Another two blocks of similar length followed at the end of the experiment – these are not discussed here as they were part of another project and are thus explained in further detail elsewhere (Stephani et al., 2022). We used an inter-stimulus-interval of 763 ms with a uniformly distributed jitter of +/– 50 ms in steps of 1 ms. Taken together, each nerve received 2000 stimuli overall. The experiment took approximately 5.5 - 6 hours, with the presentation of the experimental stimulation blocks (including breaks) taking approximately 90 minutes.

1.6: Data processing and analysis.

Unless noted otherwise, all data were analyzed using MATLAB R2019b (The MathWorks Inc., Natick, Massachusetts, USA) and the EEGlab toolbox (Delorme & Makeig, 2004).

1.6.1: Stimulation artifact removal. Electrical stimulation of peripheral nerves as employed here induces an artifact in all channels at the time point of stimulation and was removed by interpolation (using a piecewise cubic hermite interpolating polynomial). Since the temporal spread of this artifact differed among participants, as well as in cervical and lumbar channels, we defined individual artifact windows for cervical and lumbar levels by finding the beginning and the end of the artifact in the average over all trials and all cervical or lumbar ESG channels. At the cervical

level, average artifact windows ranged from -1.8 ms (SD = 0.8 ms) to 4.4 ms (SD = 1.4 ms) and at the lumbar level from -2.9 ms (SD = 1.4 ms) to 7.1 ms (SD = 2.8 ms).

1.6.2: EEG data preprocessing. First, the stimulation artifact was interpolated using the previously identified cervical artifact windows and the continuous EEG signal was down-sampled to 1000 Hz (anti-aliasing filter with cutoff at 0.9 and transition bandwidth at 0.2). *Second*, artifact sources were identified in the signals using ICA. For this, overly noisy channels were removed from the signal – based on visual inspection of the power spectral density and the trial-based root mean square activity in each channel – and interpolated (this was the case for one channel in five participants). Zero-phase IIR filtering was then applied to the continuous concatenated signal from all stimulation blocks (i.e., median and tibial nerve stimulation), consisting of a high-pass filter at 0.5 Hz and a low-pass filtered at 45 Hz (Butterworth, 4^{th} order). On the filtered signal, independent component analysis (ICA, Infomax (Makeig et al., 1995)) was performed and ICs reflecting eye blink, heart and muscle artifacts were identified. *Third*, ICs identified as representing artifactual sources were removed from the EEG signal preprocessed in the same ways as for ICA, with the difference that it i) consisted of concatenated blocks of each stimulation condition only (i.e., hand-mixed or foot-mixed) and ii) was zero-phase IIR filtered with a notch (48-53 Hz) and a band-pass (30-400 Hz) Butterworth filter of 4th order. *Fourth*, the ICA-cleaned signal was re-referenced to average reference and remaining noisy time points were identified in lower frequencies (1 - 15 Hz) using a threshold of 5 standard deviations and in higher frequencies (15 - 45 Hz) using a threshold of 60 µV. If more than 50% time points were identified in one channel, this channel was removed from the data and interpolated. In one participant 7 channels were removed from the hand-mixed condition and in another participant 18 channels were removed from the foot-mixed condition. *Fifth*, the cleaned signal was cut into epochs from 200 ms before to 700 ms after stimulus onset and baseline-corrected (with a reference interval from -110 ms to -10 ms before stimulus onset). In the hand-mixed condition, this procedure led to an average of 97.9% remaining trials (range across participants: 886 trials to 2000 trials) and in the foot-mixed condition to an average of 97.5% remaining trials (range across participants: 992 trials to 2000 trials).

1.6.3: ESG data preprocessing. After the stimulation artifact was interpolated in the individually defined cervical and lumbar artifact windows, the ESG data were down-sampled to 1000 Hz.

Since ESG data are known to present with severe cardiac artifacts (Cracco, 1973), we aimed to correct for these. In each participant, we therefore first identified R-peaks in the ECG channel using an automatic procedure provided by the FMRIB plugin for EEGlab (https://fsl.fmrib.ox.ac.uk/eeglab/fmribplugin/), which was followed by visual inspection and manual correction if necessary. Next, the heart artifact was removed from each ESG channel separately, using an approach that is a modification of a method previously developed for removing ballistocardiographic artifacts in simultaneous EEG-fMRI recordings (Niazy et al., 2005). First, a principal component analysis (PCA) was applied to a matrix of all heart artifacts (artifact x time) in one channel, with the time window of each heart artifact ranging from –0.5 * median(RR) to +0.5 * median(RR) around each R-peak (with RR referring to the interval between R-peaks, i.e., the heart-period). Then, an optimal basis set (OBS) was created based on the mean

heart artifact and the first 4 components obtained from the PCA. Finally, this OBS was fitted to each heart artifact and then removed from it.

After correction for cardiac artifacts, noisy channels were identified via visual inspection of the power spectral density and one channel in five participants was removed (no interpolation of missing channels was performed at the spinal level).

The analysis steps described below were performed in the concatenated blocks of one condition (rest, hand-mixed or foot-mixed) and, because we wanted to investigate SEPs with different references, were carried out separately for differently referenced datasets. In addition to the recording reference located over the spinous process of the 6th thoracic vertebra (TH6), we also made use of a ventrally located reference because it has been reported that this can be beneficial for SEP extraction (Desmedt & Cheron, 1981a, 1983b) – the ventral reference was channel AC in the hand-mixed and channel AL in the foot-mixed condition. *First*, a zero-phase IIR filtering was applied to the data with a notch (48-53 Hz) and a band-pass (30-400 Hz) Butterworth filter (4th order). *Second*, time points with absolute ESG activity above 100 µV were removed from the continuous data. If in one channel more than 50% of time points were identified, the whole channel was excluded instead. No further channels were removed and together with the channel exclusion based on the spectrum in the whole sample an average of 0.1 channels were removed (SD = 0.4). *Third*, the signal was cut into epochs with the same time range as reported for the EEG signal (from -200 ms to 700 ms around stimulus) and epochs were baseline-corrected (reference window -110 ms to -10 ms before stimulus onset). In the hand-mixed condition, 93.7% of trials remained in the data set on average (range across participants: 1210 trials to 2000 trials) and in the foot-mixed condition, 93.6% trials remained (range: 1193 trials to 1997 trials).

For the investigation of late potentials, the signals were pre-processed in the same way as described above, except that the reference was kept at the recording reference (at TH6) and the band-pass filter was set to 5-400 Hz.

1.6.4: ENG data preprocessing. The peripheral NAPs of interest have very short latencies (i.e., occur almost immediately after the electrical stimulation), meaning that in some participants the interpolation windows defined at the cervical or lumbar level might be too wide and thus contain the NAPs of interest. Therefore, in order to remove the stimulation artifact, but retain the NAPs, the ENG data were interpolated in a time window from 1.5 ms before to 4 ms after stimulus onset. Data were then down-sampled to 1000 Hz, band-pass and notch filtered in the same range as ESG data and cut into epochs and baseline-corrected (with the same epoch and baseline windows used for ESG data).

1.6.5: CCA. In order to enhance the signal-to-noise ratio and also allow for single-trial analysis, we made use of our multi-channel setup and applied canonical correlation analysis (CCA) to EEG and to the ventral referenced ESG data, separately for the mixed median and tibial nerve stimulation conditions. We employed a variant of CCA as used previously for single-trial extraction in EEG data (Fedele et al., 2013; Stephani et al., 2020, 2021, 2022; Waterstraat et al., 2015), also known as canonical correlation average regression (Waterstraat et al., 2015). For two multi-channel signals X and Y, CCA finds the spatial filters w_x and w_y that maximize the correlation

$$\max_{w_x, w_y} corr\left(w_x^T X, w_y^T Y\right),$$

where X is a multi-channel signal that holds all concatenated epochs from 1 to N and Y a signal that holds N times the average over all epochs concatenated (with N being the number of all epochs from one participant's recording). Both multi-channel matrices X and Y have the same size with the structure channel × time. Applied in this way, the CCA procedure serves as a template matching between the single-trial and the average of all trials. The spatial filter w_x corresponds to a spatial weighting of the multi-channel signal to separate SEP-related activity from background noise (Stephani et al., 2021). Since we were interested in early components of the SEP, we only subjected a short time window to CCA (and not the whole epoch length), namely a window from 5 ms before to 5ms after the peak of the cortical or spinal SEP component of interest. The extracted spatial filter was then applied to the whole length of the epochs. To compute the spatial activity pattern of each CCA component, the spatial filters w_x were multiplied by the covariance matrix of X in order to take the data's noise structure into account (Haufe et al., 2014). For each stimulation (median or tibial nerve stimulation), one CCA component was selected for further analyses. These components differed in the different data sets and in the different stimulation conditions: In EEG data of median nerve stimulation, the spatial pattern of the selected CCA component corresponded to the typical N20-P35 tangential dipole over the central sulcus and in EEG data of tibial nerve stimulation, it corresponded to the typical P40 radial dipole over medial somatosensory areas. In ESG data of median nerve stimulation, the spatial pattern of the selected CCA component corresponded to a radial dipole (ventral-dorsal direction) over cervical areas as typical for N13 and in ESG data of tibial nerve stimulation it corresponded to a radial dipole over lumbar areas of the spinal cord as typical for the N22. The selected component was present in all participants among the first two CCA components, i.e., those with the largest canonical correlation coefficients. Because CCA is not sensitive to the polarity of the signal, the spatial filters were multiplied by -1 if necessary, so that the extracted SEP component of interest would always result in the expected peak direction (negative for the cortical N20 and the spinal N13 in the mixed-hand condition, positive for the cortical P40 and negative for the spinal N22 in the mixed-foot condition). Note that for EEG, all channels were subjected to CCA, while for ESG only channels from the electrode patch of interest were subjected to CCA (i.e., the cervical patch in the hand-mixed condition and the lumbar patch in the foot-mixed condition).

1.6.6: Brainstem potentials. Cleaned and epoched EEG and ESG signals, which had been re-referenced during preprocessing to Fz, were combined into one dataset and referenced to a common reference at FPz, since frontal channels have been suggested for the investigation of brainstem potentials (Desmedt & Huy, 1984; Tinazzi et al., 1995; Tinazzi & Mauguière, 1995). The N14 brainstem potential following median nerve stimulation was extracted from channel SC1 and the N30 brainstem potentials following tibial nerve stimulation was extracted from channel S3 (these potentials have also been described as P14 and P30 in the literature, when using FPz as the active electrode). Please note that we also aimed to apply CCA to brainstem potentials as well, but did not succeed.

1.6.7: Potential amplitude and latency. For each participant, NAP and SEP latencies were defined individually at the peak of the potential in the average trace over all trials. At the cortical level,

SEP latency and amplitude were determined in the CCA component (Fedele et al., 2013; Stephani et al., 2020, 2021, 2022; Waterstraat et al., 2015). At the spinal level, SEP latency was determined in anatomically-defined channels (SC6 for cervical and L1 for lumbar potentials, both thoracic (TH6) referenced) and in the CCA component. Spinal amplitudes were determined in the same channels with thoracic or anterior reference as well as in the cervical or lumbar CCA component. Note that all average traces were visually inspected. In case one of the potentials was not visible in a participant, its latency was estimated based on the average latency of that potential over all participants and the amplitude was extracted at the estimated latency (Table 1 shows in the column "#" the number of participants in which potentials were detected at the individual level).

1.6.8: Statistical analysis. First, to statistically characterize the response in well-known early potentials, we tested peripheral NAP and early SEP peak-amplitudes against zero using one-sample t-tests. Second, to investigate whether we might also observe possible later-occurring potentials, cluster-based permutation testing was performed in time (from 0 to 600 ms after stimulus onset) and space (in all channels over the cervical or lumbar spine, i.e., all channels except the outermost 4 channels) using the FieldTrip toolbox (Oostenveld et al., 2011). In all analyses, significance was established at $p < 0.05$.

1.6.9: Time-frequency plots. For each participant, time-frequency analysis was performed on the averaged trial signal using a continuous short-time fast Fourier transform with a window length of 21 ms and normalized to a baseline interval from 200 ms to 10 ms before stimulus onset. The average over all participants was then displayed.

1.6.10: Signal-to-noise ratio (SNR). For all potentials, the SNR was quantified as the root-mean-square of the signal (extracted in a in a time window of +/-1 ms around the individual peak latency) divided by the root-mean-square of the noise (extracted in the same time window before the stimulus onset).

1.6.11: Assessing the robustness of spinal SEPs. In order to aid in the planning of future experiments, we assessed the robustness of spinal SEPs as a function of trial number and sample size. Towards this end, we extracted single-trial SEP amplitudes from each participant at the peak latency identified in the average over all trials of that participant, both from anatomically-defined channels (with reference at TH6) and from CCA components.

Based on these data, we carried out two analyses. *First*, we assessed the minimum number of trials to obtain a significant result at the level of a *single participant*. For each participant, a subset of trials (trial number varying between 5 and 1000 in steps of 10, including 1000) was sampled with replacement and the significance of amplitudes in the sampled trials was determined using a one-sample t-test ($p < 0.05$). This procedure was repeated 1000 times for each participant and we report the proportion of significant results for each participant. *Second*, we determined the minimum number of trials and participants to obtain a significant *group-level* effect. Therefore, we employed Monte Carlo analyses and simulated a large number of experiments (this was inspired by the approach of Boudewyn et al. (2018)). For each 'experiment', first, a subset of participants (number varying between 5, 10, 15, 20, 25, 30, 35, 36) was sampled with replacement and then a subset of trials (number varying between 5 to 1000 in steps of 10, including 1000) was sampled with

replacement. The trials were then averaged and a one-sample t-test was used to determine the significance. Each experiment was repeated 1000 times and we report the proportion of experiments that yielded a significant result (at $p < 0.05$).

Experiment 2

2.1: Participants.

26 healthy right-handed volunteers participated in this experiment. Two participants were excluded due to absent peripheral potentials in the mixed nerve stimulation condition, leading to a final sample size of 24 participants (12 female; age: 24 ± 4.5 years (mean ± SD)). All participants provided written informed consent and the study was approved by the Ethics Committee at the Medical Faculty of the University of Leipzig.

Please note that the final sample size of 24 participants was specified in a pre-registration prior to the start of the study (see section 'Open science'). This was based on a power calculation of data from of the 36 participants in Experiment 1, where we observed an effect size of d = -0.85 for median mixed nerve stimulation and of d = -0.62 for tibial mixed nerve stimulation (in 30 Hz high-pass-filtered, but otherwise uncleaned, data). Taking the smaller of these two effect sizes, and aiming for a power of 90% (at an alpha-level of 0.05 with one-tailed testing) resulted in a necessary sample size of 24 participants. Although we were using results obtained from mixed nerve stimulation as the basis for our power calculation (which is known to result in stronger responses than those from stimulation of a purely sensory nerve), we employed a conservative way to estimate our effect size: i) we used raw data that was only preprocessed by a high-pass-filter, ii) we based our power calculation on the lumbar potential that is possibly more difficult to detect, and iii) we selected the same electrode in each participant (cervical: SC6, lumbar: L1) to calculate the group statistics, which is rather conservative especially for the lumbar channels, because the location of the lumbar segments of the spinal cord differs extensively between participants (Reimann & Anson, 1944).

2.2: Experimental Design.

Similar to Experiment 1, this experiment also had a repeated-measures design, though now consisting of eight conditions, named hand-mixed, finger1, finger2, fingers1&2, foot-mixed, toe1, toe2, and toes1&2. The hand-mixed and foot-mixed conditions were the same as in Experiment 1 (except for differences in the inter-stimulus-interval and being presented completely in one block each). In the finger stimulation conditions, the index and middle finger of the participant's left hand were stimulated with electrical pulses. These pulses could occur in three different ways: to the index finger only (finger1), to the middle finger only (finger2), or to both fingers simultaneously (fingers1&2). In the toe stimulation conditions, the first and second toe of the participant's left foot were stimulated with electrical pulses either to the first toe only (toe1), to

the second toe only (toe2), or to both toes simultaneously (toes1&2). We refer to all finger and all toe stimulation conditions also as 'hand-sensory' and 'foot-sensory' conditions, because at the fingers and the toes, the median and the stimulated branches of the posterior tibial nerve contain only sensory nerve fibers. Figure 1B displays the experimental timeline of Experiment 2.

2.3: Electrical stimulation.

Equipment and electrode placement for mixed nerve stimulation was identical to what is described above for Experiment 1. For finger or toe stimulation, ring electrodes ("digital electrode for recording and stimulation", Spes Medica, Genova, Italy) were attached with the cathode being proximal to participants' left index finger and left middle finger as well as left first toe and left second toe. Each of the fingers were stimulated by a different stimulator. The stimulation intensity was set to three times the detection threshold, which was determined via the method of limits. If necessary, i.e., if participants reported to experience the stimulus as less intense over time, the stimulation intensity was slightly increased in-between stimulation blocks based on experience from pilot experiments (note that increasing the stimulus intensity has previously been reported to increase the amplitude of peripheral potentials and to improve the detection of spinal potentials (Kwast-Rabben et al., 2002)). The applied intensity was never perceived as being painful.

2.4: Electrographic recordings.

The employed recording equipment as well as the ESG, ECG and ENG electrode placement was identical to what is described above for Experiment 1. EEG was recorded using 39 electrodes arranged on an EEG cap with standard positions according to the 10-10 system and referenced to the right mastoid (RM). Recorded EEG-channels were: Fp1, Fp2, F3, F4, C3, C4, P3, P4, O1, O2, F7, F8, T7, T8, P7, P8, AFz, Fz, Cz, Pz, FC1, FC2, CP1, CP2, FC5, FC6, CP5, CP6, LM (left mastoid), FCz, C1, C2, FC3, FC4, CP3, CP4, C5, C6, and CPz. The electrooculogram was placed lateral to the outer canthi (EOGH) and in the center below (EOGV) the right eye and used the same reference as EEG. An active ground electrode was placed at POz. EMG was not recorded in this experiment.

2.5: Experimental procedure.

Since the attachment of the recording equipment to the participants and the instruction of the participants were identical to Experiment 1, in the following we only list details specific to Experiment 2. Before each experimental block started, the individual stimulation intensity was adjusted if necessary. The experiment started with 5 minutes of resting-state recording followed by 10 stimulation blocks (with short breaks between blocks). There were four different types of stimulation: i) mixed nerve stimulation of the median nerve (1 block), ii) mixed nerve stimulation of the tibial nerve (1 block), iii) sensory nerve stimulation at the fingers (4 blocks), and iv) sensory nerve stimulation at the toes (4 blocks). All blocks of one stimulation type were presented in a row

(with pauses between blocks) but the order in which the four stimulation types were presented was balanced across subjects. There was one block for hand-mixed and one block for foot-mixed stimulation and each of these blocks contained 2000 stimuli. Sensory nerve stimulation was separated into four blocks (1500 stimuli each) of finger and four blocks (1500 stimuli each) of toe stimulation. During each finger stimulation block, finger1, finger2, and fingers1&2 were stimulated in a pseudo-random order, such that each of the three stimulation conditions occurred 500 times. The same procedure was employed for the toe stimulation blocks, with the only difference that toe1, toe2, and toe12 were stimulated in pseudorandom order. Each type of digit stimulation (finger1/toe1, finger2/toe2, fingers1&2/ toes12) thus consisted of 2000 stimuli. All stimuli were delivered with an inter-stimulus-interval of 257 ms with a uniformly distributed jitter of +/- 20 ms in steps of 1 ms. The experiment took approximately 6-6.5 hours, with the presentation of the experimental blocks (including breaks) taking approximately 90 minutes.

2.6: Data processing and analysis.

The data analysis followed the analyses described in Experiment 1, except that in addition to the hand-mixed and foot-mixed conditions, there were also the hand-sensory (finger1, finger2, fingers1&2) and foot-sensory (toe1, toe2, toes1&2) conditions.

2.6.1: Stimulation artifact removal. Identical to Experiment 1, we defined individual artifact windows in cervical and lumbar ESG channels. At the cervical level, average artifact windows ranged from -2.0 ms (std = 1.1 ms) to 4.2 ms (std = 1.8 ms) and at the lumbar level from -2.0 ms (std = 1.1 ms) to 4.8 ms (std = 2.0 ms).

2.6.2: EEG data preprocessing. EEG preprocessing was performed in the same way as described above for Experiment 1. One noisy channel was identified in each of 6 participants and interpolated before ICA. One difference to the EEG analysis described in Experiment 1 was that in step three the ICs identified as representing artifactual sources were removed from the EEG signal that i) consisted of concatenated blocks of each stimulation condition only (i.e., hand-mixed, foot-mixed, hand sensory, or foot-sensory) and ii) had zero-phase IIR filtering applied with a 50-Hz comb filter (40th order, bandwidth 0.003) and a band-pass (30-400 Hz) Butterworth filter (4th order); the change in filtering was due to additional line noise and its harmonics introduced by electrical stimulation via ring electrodes. Identical to Experiment 1, noisy time points were removed, but here this did not result in the exclusion of additional channels. In Experiment 2, epochs were cut from 200 ms before to 300 ms after stimulus onset and baseline-corrected (with a reference interval from -110 ms to -10 ms before stimulus onset). Across conditions, this procedure resulted in the following number of trials remaining on average: hand-sensory 99.5% (range across participants: 5795 trials to 6000 trials), hand-mixed 99.4% (range across participants: 1921 trials to 2000 trials), foot-sensory 99.2% (range across participants: 5678 trials to 6000 trials), and foot-mixed 99.8% (range across participants: 1978 trials to 2000 trials).

2.6.3: ESG data preprocessing. Since ESG data were preprocessed the same way as described in Experiment 1, only the differences are listed in the following. After cardiac artifact correction, an average of 1.8 channels (std = 1.0) were removed in four participants. Due to the use of ring

electrodes for digit stimulation, more line noise and its harmonics were visible in the data. Therefore, zero-phase IIR filtering was applied with a 50-Hz comb filter (40th order, bandwidth 0.003) and a band-pass (30-400 Hz) Butterworth filter (4th order). Similarly to Experiment 1, time points with ESG activity above 100 µV were removed from the continuous data, and if more than 50% of data points were removed from a channel, the whole channel was excluded instead. In one participant, two additional channels were removed. The signal was cut into epochs with the same time range as reported for the EEG signal (from -200 ms to to 300 ms around stimulus onset) and epochs were baseline-corrected (reference window -110 ms to -10 ms before stimulus onset). On average, 91.3% of trials remained in the hand-mixed condition (range across participants: 999 trials to 2000 trials), 90.5% of trials remained in the hand-sensory conditions (range across participants: 3873 trials to 5993 trials), 94.2% of trials remained in the foot-mixed condition (range across participants: 1433 trials to 2000 trials), and 91.4% of trials remained in the foot-sensory conditions (range across participants: 3751 trials to 5988 trials).

2.6.4: ENG data preprocessing. ENG data were processed the same way as described for Experiment 1 above.

2.6.5: CCA. CCA was trained in the same way as explained above for Experiment 1. More specifically, it was trained on data from mixed nerve conditions (due to their higher SNR) and the spatial filters were then applied to the respective mixed and sensory nerve conditions.

2.6.6: Brainstem potentials. We did not investigate brainstem potentials in Experiment 2 due to the lower SNR of SEPs after sensory nerve stimulation.

2.6.7: Potential amplitude and latency. These metrics were calculated in identical fashion as described for Experiment 1.

2.6.8: Statistical Methods. SEP amplitudes from all experimental conditions were compared against zero using one-sample t-tests. SEP amplitudes and latencies in mixed and sensory conditions were compared using paired t-tests. To balance the number of stimuli for mixed and sensory conditions only the double stimulation conditions were subjected to this statistical comparison.

1.6.9: Signal-to-noise ratio (SNR). For all potentials, the SNR was quantified as the root-mean-square of the signal (extracted in a in a time window of +/-1 ms around the individual peak latency) divided by the root-mean-square of the noise (extracted in the same time window before the stimulus onset).

2.6.10: Assessing the robustness of spinal SEPs. In order to also assess the robustness of the spinal SEPs elicited by sensory nerve stimulation, we repeated the same analyses as outlined for Experiment 1, though this time for the conditions finger1, finger2, fingers1&2, toe1, toe2, and toes1&2). Please note that we adjusted the number of participants (number varying between 5, 10, 15, 20, 24) according to the smaller sample size of Experiment 2.

2.6.11: Linear-mixed-effects models across somatosensory processing levels. To examine whether electrophysiological signals covaried across different stages of somatosensory processing, we employed linear-mixed-effects (LME) models. Specifically, we tested whether the effect of

stimulation condition (mixed nerve, finger/toe1, finger/toe2, fingers/toes1&2) on signal amplitude propagated through the somatosensory processing hierarchy. For this, we used random-intercept LME models with the random factor subject, and in- or excluding the factor stimulation condition (with mixed nerve as reference level) to the regressions of peak amplitudes on consecutive somatosensory processing levels in the following way:

$$spinal\ cord \sim 1 + periphery + (1 \mid subject)$$

$$spinal\ cord \sim 1 + periphery * condition + (1 \mid subject)$$

$$S1 \sim 1 + spinal\ cord + (1 \mid subject)$$

$$S1 \sim 1 + spinal\ cord * condition + (1 \mid subject)\ .$$

These analyses were separately performed for stimulation conditions of the hand and the foot. Variables 'spinal cord' and 'S1' correspond to the single-trial peak amplitudes of the respective signals extracted using CCA as explained in the methods section "2.6.5: CCA", and 'periphery' to the peripheral single-trial NAP peak amplitude measured at the axilla or popliteal fossa in hand and foot stimulation, respectively (in foot stimulation, the signal was derived from the knee electrode with the largest evoked potential). All amplitude measures were z-transformed before including them in the LME models. The fixed-effect coefficients were estimated based on the maximum likelihood (ML) and p values of the fixed-effect coefficients were obtained adjusting the denominator degrees of freedom according to Satterthwaite's method (Satterthwaite, 1946). The LME models were calculated in R (version 4.2.0, R Core Team, 2018) with the lmer function of the lme4 package (version 1.1-30, Bates et al., 2015), as well as including the lmerTest package (version 3.1-3 (Kuznetsova et al., 2017)) for the implementation of the Satterthwaite method.

2.6.12: Interaction ratio. If the information from the simultaneous stimulation of two digits (fingers or toes) is integrated at a certain neural processing stage, then the SEP amplitude following this simultaneous digit stimulation should be reduced compared to arithmetic sum of the SEP amplitudes following separate stimulation of the two digits. To quantify this attenuation effect for each participant, we calculated an interaction ratio (IR) as suggested previously (Cataldo et al., 2019; Hsieh et al., 1995; Ruben et al., 2006). The IR captures the amplitude attenuation caused by the simultaneous stimulation of two digits and describes this attenuation as percentage of the expected amplitude sum of single-digit stimulations:

$$IR = (\sum(D1,D2) - D1D2) / \sum(D1,D2) * 100$$

where ∑(D1,D2) is the sum over SEP (or NAP) amplitudes following single-digit (finger/toe1 or finger/toe2) stimulation and D1D2 the SEP (or NAP) amplitude following double-digit stimulation (fingers/toes1&2). A positive IR would reflect the percentage of SEP amplitude attenuation from the expected amplitude (i.e., the sum of SEP amplitudes to single-digit stimulation) and an IR of 0% would suggest that there is no integration happening, meaning SEP amplitudes to double-digit and the sum of single-digit stimulations have the same size (a negative IR would mean that there

is an amplification effect of SEP amplitudes to double-digit stimulation). IR values from each participant to finger and toe stimulation were tested against zero using one-sample t-tests.

Open science

Both studies were pre-registered on the Open Science Framework before the start of data acquisition and the pre-registrations are openly available (see https://osf.io/sgptz and https://osf.io/mjdha); differences between the analyses suggested in the pre-registrations and the analyses carried out here are listed in the Supplementary Material. All data have been uploaded in EEG-BIDS format (Gorgolewski et al., 2016; Pernet et al., 2019) to OpenNeuro and are openly available (see https://doi.org/10.18112/openneuro.ds003891.v1.0.0 and https://doi.org/10.18112/openneuro.ds003889.v1.0.0). Please note that currently, only the reviewers of this manuscript have access to the data – the data will be made publicly available upon acceptance of the manuscript in a journal. All analysis code has been deposited on Github and is openly available (see https://github.com/eippertlab/spinal_sep1 and https://github.com/eippertlab/spinal_sep2).

Acknowledgements

We would like to thank Ulrike Horn for providing the code that allowed for manual correction of automatically detected R-peaks. We would further like to thank our student research assistants Janek Haschke, Pia-Lena Baisch, Paula Kosel, Max Braune, Samuel Simeon, and Marleen Löffler for their help in recruitment and data acquisition.

Funding information

FE received funding from the Max Planck Society and the European Research Council (under the European Union's Horizon 2020 research and innovation programme; grant agreement No 758974).

Competing interest

The authors declare no competing financial or non-financial interests.

References

Abraira, V. E., & Ginty, D. D. (2013). The Sensory Neurons of Touch. *Neuron*, *79*(4), 618–639. https://doi.org/10.1016/j.neuron.2013.07.051

Abraira, V. E., Kuehn, E. D., Chirila, A. M., Springel, M. W., Toliver, A. A., Zimmerman, A. L., Orefice, L. L., Boyle, K. A., Bai, L., Song, B. J., Bashista, K. A., O'Neill, T. G., Zhuo, J., Tsan, C., Hoynoski, J., Rutlin, M., Kus, L., Niederkofler, V., Watanabe, M., … Ginty, D. D. (2017). The Cellular and Synaptic Architecture of the Mechanosensory Dorsal Horn. *Cell*, *168*(1–2), 295-310.e19. https://doi.org/10.1016/j.cell.2016.12.010

Akaza, M., Kawabata, S., Ozaki, I., Miyano, Y., Watanabe, T., Adachi, Y., Sekihara, K., Sumi, Y., & Yokota, T. (2021). Noninvasive measurement of sensory action currents in the

cervical cord by magnetospinography. *Clinical Neurophysiology*, *132*(2), 382–391. https://doi.org/10.1016/j.clinph.2020.11.029

Barry, R. L., Vannesjo, S. J., By, S., Gore, J. C., & Smith, S. A. (2018). Spinal cord MRI at 7T. *NeuroImage*, *168*, 437–451. https://doi.org/10.1016/j.neuroimage.2017.07.003

Bates, D., Mächler, M., Bolker, B., & Walker, S. (2015). Fitting Linear Mixed-Effects Models Using lme4. *Journal of Statistical Software*, *67*(1). https://doi.org/10.18637/jss.v067.i01

Beall, J. E., Applebaum, A. E., Foreman, R. D., & Willis, W. D. (1977). Spinal cord potentials evoked by cutaneous afferents in the monkey. *Journal of Neurophysiology*, *40*(2), 199–211. https://doi.org/10.1152/jn.1977.40.2.199

Berić, A. (1988). Stability of lumbosacral somatosensory evoked potentials in a long-term follow-up. *Muscle & Nerve*, *11*(6), 6. https://doi.org/10.1002/mus.880110615

Biermann, K., Schmitz, F., Witte, O. W., Konczak, J., Freund, H.-J., & Schnitzler, A. (1998). Interaction of finger representation in the human first somatosensory cortex: A neuromagnetic study. *Neuroscience Letters*, *251*(1), 13–16. https://doi.org/10.1016/S0304-3940(98)00480-7

Boehme, R., Hauser, S., Gerling, G. J., Heilig, M., & Olausson, H. (2019). Distinction of self-produced touch and social touch at cortical and spinal cord levels. *Proceedings of the National Academy of Sciences*, *116*(6), 6. https://doi.org/10.1073/pnas.1816278116

Boudewyn, M. A., Luck, S. J., Farrens, J. L., & Kappenman, E. S. (2018). How many trials does it take to get a significant ERP effect? It depends. *Psychophysiology*, *55*(6), e13049. https://doi.org/10.1111/psyp.13049

Brown, A. G. (1981). *Organization in the Spinal Cord*. Springer London. https://doi.org/10.1007/978-1-4471-1305-8

1364 Button, K. S., Ioannidis, J. P. A., Mokrysz, C., Nosek, B. A., Flint, J., Robinson, E. S. J., & Munafò,
1365 M. R. (2013). Power failure: Why small sample size undermines the reliability of
1366 neuroscience. *Nature Reviews Neuroscience*, *14*(5), 365–376.
1367 https://doi.org/10.1038/nrn3475
1368 Cadotte, D. W., Cadotte, A., Cohen-Adad, J., Fleet, D., Livne, M., Wilson, J. R., Mikulis, D.,
1369 Nugaeva, N., & Fehlings, M. G. (2015). Characterizing the Location of Spinal and
1370 Vertebral Levels in the Human Cervical Spinal Cord. *American Journal of*
1371 *Neuroradiology*, *36*(4), 803–810. https://doi.org/10.3174/ajnr.A4192
1372 Cataldo, A., Ferrè, E. R., di Pellegrino, G., & Haggard, P. (2019). Why the whole is more than the
1373 sum of its parts: Salience-driven overestimation in aggregated tactile sensations. *Quarterly*
1374 *Journal of Experimental Psychology*, *72*(10), 2509–2526.
1375 https://doi.org/10.1177/1747021819847131
1376 Chander, B. S., Deliano, M., Azañón, E., Büntjen, L., & Stenner, M.-P. (2022). Non-invasive
1377 recording of high-frequency signals from the human spinal cord. *NeuroImage*, *253*,
1378 119050. https://doi.org/10.1016/j.neuroimage.2022.119050
1379 Ciccarelli, O., Cohen, J. A., Reingold, S. C., Weinshenker, B. G., Amato, M. P., Banwell, B.,
1380 Barkhof, F., Bebo, B., Becher, B., Bethoux, F., Brandt, A., Brownlee, W., Calabresi, P.,
1381 Chatway, J., Chien, C., Chitnis, T., Ciccarelli, O., Cohen, J., Comi, G., … Xu, J. (2019).
1382 Spinal cord involvement in multiple sclerosis and neuromyelitis optica spectrum disorders.
1383 *The Lancet Neurology*, *18*(2), 185–197. https://doi.org/10.1016/S1474-4422(18)30460-5
1384 Cohen, L. G., & Starr, A. (1985). Vibration and muscle contraction affect somatosensory evoked
1385 potentials. *Neurology*, *35*(5), 5. https://doi.org/10.1212/WNL.35.5.691

1386 Cohen-Adad, J. (2017). Functional Magnetic Resonance Imaging of the Spinal Cord: Current
1387 Status and Future Developments. *Seminars in Ultrasound, CT and MRI*, *38*(2), 176–186.
1388 https://doi.org/10.1053/j.sult.2016.07.007
1389 Cracco, R. Q. (1972). The initial positive potential of the human scalp-recorded somatosensory
1390 evoked response. *Electroencephalography and Clinical Neurophysiology*, *32*(6), 6.
1391 https://doi.org/10.1016/0013-4694(72)90099-5
1392 Cracco, R. Q. (1973). Spinal evoked response: Peripheral nerve stimulation in man.
1393 *Electroencephalography and Clinical Neurophysiology*, *35*(4), 4.
1394 https://doi.org/10.1016/0013-4694(73)90195-8
1395 Cruccu, G., Aminoff, M. J., Curio, G., Guerit, J. M., Kakigi, R., Mauguiere, F., Rossini, P. M.,
1396 Treede, R.-D., & Garcia-Larrea, L. (2008). Recommendations for the clinical use of
1397 somatosensory-evoked potentials. *Clinical Neurophysiology*, *119*(8), 1705–1719.
1398 https://doi.org/10.1016/j.clinph.2008.03.016
1399 Curio, G., Erne, S. N., Sandfort, J., Scheer, J., Stehr, R., & Trahms, L. (1991). Exploratory
1400 mapping of evoked neuromagnetic activity from human peripheral nerve, brachial plexus
1401 and spinal cord. *Electroencephalography and Clinical Neurophysiology*, *81*, 450–453.
1402 Delbeke, J., McComas, A. J., & Kopec, S. J. (1978). Analysis of evoked lumbosacral potentials in
1403 man. *Journal of Neurology, Neurosurgery & Psychiatry*, *41*(4), 4.
1404 https://doi.org/10.1136/jnnp.41.4.293
1405 Delorme, A., & Makeig, S. (2004). EEGLAB: An open source toolbox for analysis of single-trial
1406 EEG dynamics including independent component analysis. *Journal of Neuroscience*
1407 *Methods*, *134*(1), 9–21. https://doi.org/10.1016/j.jneumeth.2003.10.009

1408 Desmedt, J. E. (1985). Critical neuromonitoring at spinal and brainstem levels by somatosensory
1409 evoked potentials. *Central Nervous System Trauma: Journal of the American Paralysis*
1410 *Association*, *2*(3), 169–186. https://doi.org/10.1089/cns.1985.2.169
1411 Desmedt, J. E., & Cheron, G. (1981). Prevertebral (oesophageal) recording of subcortical
1412 somatosensory evoked potentials in man: The spinal P13 component and the dual nature
1413 of the spinal generators. *Electroencephalography and Clinical Neurophysiology*, *52*(4), 4.
1414 https://doi.org/10.1016/0013-4694(81)90055-9
1415 Desmedt, J. E., & Cheron, G. (1983). Spinal and far-field components of human somatosensory
1416 evoked potentials to posterior tibial nerve stimulation analysed with oesophageal
1417 derivations and non-cephalic reference recording. *Electroencephalography and Clinical*
1418 *Neurophysiology*, *56*(6), 6. https://doi.org/10.1016/0013-4694(83)90031-7
1419 Desmedt, J. E., & Huy, N. T. (1984). BIT-mapped colour imaging of the potential fields of
1420 propagated and segmental subcortical components of somatosensory evoked potentials in
1421 man. *Electroencephalography and Clinical Neurophysiology*, *58*(6), 6.
1422 https://doi.org/10.1016/0013-4694(84)90037-3
1423 Di Pietro, G., Di Stefano, G., Leone, C., Di Lionardo, A., Sgro, E., Blockeel, A. J., Caspani, O.,
1424 Garcia-Larrea, L., Mouraux, A., Phillips, K. G., Treede, R.-D., Valeriani, M., & Truini, A.
1425 (2021). The N13 spinal component of somatosensory evoked potentials is modulated by
1426 heterotopic noxious conditioning stimulation suggesting an involvement of spinal wide
1427 dynamic range neurons. *Neurophysiologie Clinique*, *51*(6), 517–523.
1428 https://doi.org/10.1016/j.neucli.2021.09.001
1429 Dimitrijevic, M. R., Larsson, L. E., Lehmkuhl, D., & Sherwood, A. (1978). Evoked spinal cord
1430 and nerve root potentials in humans using a non-invasive recording technique.

Electroencephalography and Clinical Neurophysiology, *45*(3), 3. https://doi.org/10.1016/0013-4694(78)90185-2

Dimitrijevic, M. R., Lehmkuhl, L. D., Sedgwick, E. M., Sherwood, A. M., & McKay, W. B. (1980). Characteristics of Spinal Cord-Evoked Responses in Man. *Stereotactic and Functional Neurosurgery*, *43*(3–5), 3–5. https://doi.org/10.1159/000102245

Dykest, R. W., & Terzis, J. K. (1981). Spinal nerve distributions in the upper Limb: The organization of the dermatome and afferent myotome. *Philosophical Transactions of the Royal Society of London. B, Biological Sciences*, *293*(1070), 509–554. https://doi.org/10.1098/rstb.1981.0083

El-Negamy, E., & Sedgwick, E. M. (1978). Properties of a spinal somatosensory evoked potential recorded in man. *Journal of Neurology, Neurosurgery & Psychiatry*, *41*(8), 762–768. https://doi.org/10.1136/jnnp.41.8.762

Emerson, R. G., Seyal, M., & Pedley, T. A. (1984). Somatosensory evoked potentials following median nerve stimulation: I. The cervical components. *Brain*, *107*(1), 1. https://doi.org/10.1093/brain/107.1.169

Ertekin, C. (1976). Studies on the human evoked electrospinogram. I. The origin of the segmental evoked potentials. *Acta Neurologica Scandinavica*, *53*(1), 1. https://doi.org/10.1111/j.1600-0404.1976.tb04321.x

Fabbrini, A., Guerra, A., Giangrosso, M., Manzo, N., Leodori, G., Pasqualetti, P., Conte, A., Di Lazzaro, V., & Berardelli, A. (2022). Transcranial alternating current stimulation modulates cortical processing of somatosensory information in a frequency- and time-specific manner. *NeuroImage*, *254*, 119119. https://doi.org/10.1016/j.neuroimage.2022.119119

1454 Fedele, T., Scheer, H.-J., Burghoff, M., Waterstraat, G., Nikulin, V. V., & Curio, G. (2013).
1455 Distinction between added-energy and phase-resetting mechanisms in non-invasively
1456 detected somatosensory evoked responses. *2013 35th Annual International Conference of*
1457 *the IEEE Engineering in Medicine and Biology Society (EMBC)*, 1688–1691.
1458 https://doi.org/10.1109/EMBC.2013.6609843
1459 Finsterbusch, J., Sprenger, C., & Büchel, C. (2013). Combined T2*-weighted measurements of
1460 the human brain and cervical spinal cord with a dynamic shim update. *NeuroImage*, *79*,
1461 153–161. https://doi.org/10.1016/j.neuroimage.2013.04.021
1462 Gandevia, S. C., Burke, D., & McKeon, B. B. (1983). Convergence in the somatosensory pathway
1463 between cutaneous afferents from the index and middle fingers in man. *Experimental Brain*
1464 *Research*, *50–50*(2–3). https://doi.org/10.1007/BF00239208
1465 Gasser, H. S., & Graham, H. T. (1933). Potentials produced in the spinal cord by stimulation of
1466 dorsal roots. *American Journal of Physiology-Legacy Content*, *103*(2), 303–320.
1467 https://doi.org/10.1152/ajplegacy.1933.103.2.303
1468 Giesler, G. J., Nahin, R. L., & Madsen, A. M. (1984). Postsynaptic dorsal column pathway of the
1469 rat. I. Anatomical studies. *Journal of Neurophysiology*, *51*(2), 260–275.
1470 https://doi.org/10.1152/jn.1984.51.2.260
1471 Gilmore, R. L., Bass, N. H., Wright, E. A., Greathouse, D., Stanback, K., & Norvell, E. (1985).
1472 Developmental assessment of spinal cord and cortical evoked potentials after tibial nerve
1473 stimulation: Effects of age and stature on normative data during childhood.
1474 *Electroencephalography and Clinical Neurophysiology/Evoked Potentials Section*, *62*(4),
1475 4. https://doi.org/10.1016/0168-5597(85)90002-4

1476 Gorgolewski, K. J., Auer, T., Calhoun, V. D., Craddock, R. C., Das, S., Duff, E. P., Flandin, G.,
1477 Ghosh, S. S., Glatard, T., Halchenko, Y. O., Handwerker, D. A., Hanke, M., Keator, D.,
1478 Li, X., Michael, Z., Maumet, C., Nichols, B. N., Nichols, T. E., Pellman, J., … Poldrack,
1479 R. A. (2016). The brain imaging data structure, a format for organizing and describing
1480 outputs of neuroimaging experiments. *Scientific Data*, *3*(1), 160044.
1481 https://doi.org/10.1038/sdata.2016.44
1482 Häring, M., Zeisel, A., Hochgerner, H., Rinwa, P., Jakobsson, J. E. T., Lönnerberg, P., La Manno,
1483 G., Sharma, N., Borgius, L., Kiehn, O., Lagerström, M. C., Linnarsson, S., & Ernfors, P.
1484 (2018). Neuronal atlas of the dorsal horn defines its architecture and links sensory input to
1485 transcriptional cell types. *Nature Neuroscience*, *21*(6), 869–880.
1486 https://doi.org/10.1038/s41593-018-0141-1
1487 Hashimoto, J., Kawabata, S., Sasaki, T., Hoshino, Y., Sekihara, K., Adachi, Y., Watanabe, T.,
1488 Miyano, Y., Mitani, Y., Sato, S., Kim, S., Yoshii, T., & Okawa, A. (2022). Assessment of
1489 thoracic spinal cord electrophysiological activity through magnetoneurography. *Clinical*
1490 *Neurophysiology*, *133*, 39–47. https://doi.org/10.1016/j.clinph.2021.09.023
1491 Haufe, S., Meinecke, F., Görgen, K., Dähne, S., Haynes, J.-D., Blankertz, B., & Bießmann, F.
1492 (2014). On the interpretation of weight vectors of linear models in multivariate
1493 neuroimaging. *NeuroImage*, *87*, 96–110.
1494 https://doi.org/10.1016/j.neuroimage.2013.10.067
1495 Hochman, S. (2007). Spinal cord. *Current Biology*, *17*(22), R950–R955.
1496 https://doi.org/10.1016/j.cub.2007.10.014
1497 Hoechstetter, K., Rupp, A., Stančák, A., Meinck, H.-M., Stippich, C., Berg, P., & Scherg, M.
1498 (2001). Interaction of Tactile Input in the Human Primary and Secondary Somatosensory

1499 Cortex—A Magnetoencephalographic Study. *NeuroImage*, *14*(3), 759–767.
1500 https://doi.org/10.1006/nimg.2001.0855

1501 Hsieh, C.-L., Shima, F., Tobimatsu, S., Sun, S.-J., & Kato, M. (1995). The interaction of the
1502 somatosensory evoked potentials to simultaneous finger stimuli in the human central
1503 nervous system. A study using direct recordings. *Electroencephalography and Clinical*
1504 *Neurophysiology/Evoked Potentials Section*, *96*(2), 135–142.
1505 https://doi.org/10.1016/0168-5597(94)00251-9

1506 Huttunen, J., Ahlfors, S., & Hari, R. (1992). Interaction of afferent impulses in the human primary
1507 sensorimotor cortex. *Electroencephalography and Clinical Neurophysiology*, *82*(3), 176–
1508 181. https://doi.org/10.1016/0013-4694(92)90165-e

1509 Ishibashi, H., Tobimatsu, S., Shigeto, H., Morioka, T., Yamamoto, T., & Fukui, M. (2000).
1510 Differential interaction of somatosensory inputs in the human primary sensory cortex: A
1511 magnetoencephalographic study. *Clinical Neurophysiology*, *111*(6), 1095–1102.
1512 https://doi.org/10.1016/S1388-2457(00)00266-2

1513 Jiang, N., Wang, L., Huang, Z., & Li, G. (2021). Mapping Responses of Lumbar Paravertebral
1514 Muscles to Single-Pulse Cortical TMS Using High-Density Surface Electromyography.
1515 *IEEE Transactions on Neural Systems and Rehabilitation Engineering*, *29*, 831–840.
1516 https://doi.org/10.1109/TNSRE.2021.3076095

1517 Jones, S. J. (1977). Short latency potentials recorded from the neck and scalp following median
1518 nerve stimulation in man. *Electroencephalography and Clinical Neurophysiology*, *43*(6),
1519 6. https://doi.org/10.1016/0013-4694(77)90008-6

1520 Kinany, N., Pirondini, E., Micera, S., & Van De Ville, D. (2022). Spinal Cord fMRI: A New
1521 Window into the Central Nervous System. *The Neuroscientist*, 107385842211018.
1522 https://doi.org/10.1177/10738584221101827
1523 Kuner, R., & Flor, H. (2017). Structural plasticity and reorganisation in chronic pain. *Nature*
1524 *Reviews Neuroscience*, *18*(1), 20–30. https://doi.org/10.1038/nrn.2016.162
1525 Kuznetsova, A., Brockhoff, P. B., & Christensen, R. H. B. (2017). lmerTest Package: Tests in
1526 Linear Mixed Effects Models. *Journal of Statistical Software*, *82*(13).
1527 https://doi.org/10.18637/jss.v082.i13
1528 Kwast-Rabben, O., Libelius, R., & Heikkilä, H. (2002). Somatosensory evoked potentials
1529 following stimulation of digital nerves: SEP from Digital Nerves. *Muscle & Nerve*, *26*(4),
1530 533–538. https://doi.org/10.1002/mus.10237
1531 Landelle, C., Lungu, O., Vahdat, S., Kavounoudias, A., Marchand-Pauvert, V., De Leener, B., &
1532 Doyon, J. (2021). Investigating the human spinal sensorimotor pathways through
1533 functional magnetic resonance imaging. *NeuroImage*, *245*, 118684.
1534 https://doi.org/10.1016/j.neuroimage.2021.118684
1535 Lastimosa, A. C. B., Bass, N. H., Stanback, K., & Norvell, E. E. (1982). Lumbar spinal cord and
1536 early cortical evoked potentials after tibial nerve stimulation: Effects of stature on
1537 normative data. *Electroencephalography and Clinical Neurophysiology*, *54*(5), 5.
1538 https://doi.org/10.1016/0013-4694(82)90035-9
1539 Le Bars, D., & Cadden, S. W. (2008). What is a Wide-Dynamic-Range Cell? In *The Senses: A*
1540 *Comprehensive Reference* (pp. 331–338). Elsevier. https://doi.org/10.1016/B978-
1541 012370880-9.00167-5

1542 Lee, M. W. L., McPhee, R. W., & Stringer, M. D. (2008). An evidence-based approach to human
1543 dermatomes. *Clinical Anatomy*, *21*(5), 363–373. https://doi.org/10.1002/ca.20636
1544 Li, L., Rutlin, M., Abraira, V. E., Cassidy, C., Kus, L., Gong, S., Jankowski, M. P., Luo, W.,
1545 Heintz, N., Koerber, H. R., Woodbury, C. J., & Ginty, D. D. (2011). The Functional
1546 Organization of Cutaneous Low-Threshold Mechanosensory Neurons. *Cell*, *147*(7), 1615–
1547 1627. https://doi.org/10.1016/j.cell.2011.11.027
1548 Liberson, W. T., Gratzer, M., Zalis, A., & Grabinski, B. (1966). Comparison of conduction
1549 velocities of motor and sensory fibers determined by different methods. *Archives of*
1550 *Physical Medicine and Rehabilitation*, *47*(1), 1.
1551 Liu, Y., Latremoliere, A., Li, X., Zhang, Z., Chen, M., Wang, X., Fang, C., Zhu, J., Alexandre, C.,
1552 Gao, Z., Chen, B., Ding, X., Zhou, J.-Y., Zhang, Y., Chen, C., Wang, K. H., Woolf, C. J.,
1553 & He, Z. (2018). Touch and tactile neuropathic pain sensitivity are set by corticospinal
1554 projections. *Nature*, *561*(7724), 547–550. https://doi.org/10.1038/s41586-018-0515-2
1555 Lopes da Silva, F. (2013). EEG and MEG: Relevance to Neuroscience. *Neuron*, *80*(5), 1112–1128.
1556 https://doi.org/10.1016/j.neuron.2013.10.017
1557 Maccabee, P. J., Pinkhasov, E. I., & Cracco, R. Q. (1983). Short latency somatosensory evoked
1558 potentials to median nerve stimulation: Effect of low frequency filter.
1559 *Electroencephalography and Clinical Neurophysiology*, *55*(1), 1.
1560 https://doi.org/10.1016/0013-4694(83)90144-X
1561 Magladery, J. W., Porter, W. E., Park, A. M., & Teasdall, R. D. (1951). Electrophysiological
1562 studies of nerve and reflex activity in normal man. IV. The two-neurone reflex and
1563 identification of certain action potentials from spinal roots and cord. *Bulletin of the Johns*
1564 *Hopkins Hospital*, *88*, 499–519.

1565 Makeig, S., Bell, A., Jung, T.-P., & Sejnowski, T. J. (1995). Independent Component Analysis of
1566 Electroencephalographic Data. In D. Touretzky, M. C. Mozer, & M. Hasselmo (Eds.),
1567 *Advances in Neural Information Processing Systems* (Vol. 8). MIT Press.
1568 https://proceedings.neurips.cc/paper/1995/file/754dda4b1ba34c6fa89716b85d68532b-
1569 Paper.pdf
1570 Mardell, L. C., O'Neill, G. C., Tierney, T. M., Timms, R. C., Zich, C., Barnes, G. R., & Bestmann,
1571 S. (2022). *Concurrent spinal and brain imaging with optically pumped magnetometers*
1572 [Preprint]. Neuroscience. https://doi.org/10.1101/2022.05.12.491623
1573 Matthews, W. B., Beauchamp, M., & Small, D. G. (1974). Cervical somato-sensory evoked
1574 responses in man. *Nature*, *252*(5480), 5480. https://doi.org/10.1038/252230a0
1575 Mauguière, F. (1996). Clinical utility of somatosensory evoked potentials (SEPs): Present debates
1576 and future trends. *Electroencephalography and Clinical Neurophysiology. Supplement*, *46*,
1577 27–33.
1578 Mauguière, F. (2000). Anatomic Origin of the Cervical N13 Potential Evoked by Upper Extremity
1579 Stimulation: *Journal of Clinical Neurophysiology*, *17*(3), 236–245.
1580 https://doi.org/10.1097/00004691-200005000-00002
1581 Mauguière, F., Allison, T., Babiloni, C., Buchner, H., Eisen, A. A., Goodin, D. S., Jones, S. J.,
1582 Kakigi, R., Matsuoka, S., Nuwer, M., Rossini, P. M., & Shibasaki, H. (1999).
1583 Somatosensory evoked potentials. The International Federation of Clinical
1584 Neurophysiology. *Electroencephalography and Clinical Neurophysiology. Supplement*,
1585 *52*, 79–90.

McKay, W. B., & Galloway, B. L. (1979). Technological Aspects of Recording Evoked Potentials from the Cauda Equina and Lumbosacral Spinal Cord in Man. *American Journal of EEG Technology*, *19*(2), 2. https://doi.org/10.1080/00029238.1979.11079968

McPherson, J. G., & Bandres, M. F. (2021). Spontaneous neural synchrony links intrinsic spinal sensory and motor networks during unconsciousness. *ELife*, *10*, e66308. https://doi.org/10.7554/eLife.66308

Michel, C. M., & Murray, M. M. (2012). Towards the utilization of EEG as a brain imaging tool. *NeuroImage*, *61*(2), 371–385. https://doi.org/10.1016/j.neuroimage.2011.12.039

Mizutani, Y., & Kuriki, S. (1986). Somatically Evoked Magnetic Fields in the Vicinity of the Neck. *IEEE Transactions on Biomedical Engineering*, *BME-33*(5), 510–516. https://doi.org/10.1109/TBME.1986.325738

Niazy, R. K., Beckmann, C. F., Iannetti, G. D., Brady, J. M., & Smith, S. M. (2005). Removal of FMRI environment artifacts from EEG data using optimal basis sets. *NeuroImage*, *28*(3), 720–737. https://doi.org/10.1016/j.neuroimage.2005.06.067

Okajima, Y., Chino, N., Saitoh, E., & Kimura, A. (1991). Interactions of somatosensory evoked potentials: Simultaneous stimulation of two nerves. *Electroencephalography and Clinical Neurophysiology/Evoked Potentials Section*, *80*(1), 26–31. https://doi.org/10.1016/0168-5597(91)90039-z

Oostenveld, R., Fries, P., Maris, E., & Schoffelen, J.-M. (2011). FieldTrip: Open Source Software for Advanced Analysis of MEG, EEG, and Invasive Electrophysiological Data. *Computational Intelligence and Neuroscience*, *2011*, 1–9. https://doi.org/10.1155/2011/156869

1608 Pernet, C. R., Appelhoff, S., Gorgolewski, K. J., Flandin, G., Phillips, C., Delorme, A., &
1609 Oostenveld, R. (2019). EEG-BIDS, an extension to the brain imaging data structure for
1610 electroencephalography. *Scientific Data*, *6*(1). https://doi.org/10.1038/s41597-019-0104-8
1611 Pratt, H., & Starr, A. (1981). Mechanically and electrically evoked somatosensory potentials in
1612 humans: Scalp and neck distributions of short latency components.
1613 *Electroencephalography and Clinical Neurophysiology*, *51*(2), 2.
1614 https://doi.org/10.1016/0013-4694(81)90002-X
1615 Pratt, H., Starr, A., Amlie, R. N., & Politoske, D. (1979). Mechanically and electrically evoked
1616 somatosensory potentials in normal humans. *Neurology*, *29*(9, Part 1), 1236–1236.
1617 https://doi.org/10.1212/WNL.29.9_Part_1.1236
1618 R Core Team. (2018). *R: A Language and Environment for Statistical Computing*. R Foundation
1619 for Statistical Computing, Vienna. https://www.R-project.org
1620 Ran, C., Hoon, M. A., & Chen, X. (2016). The coding of cutaneous temperature in the spinal cord.
1621 *Nature Neuroscience*, *19*(9), 1201–1209. https://doi.org/10.1038/nn.4350
1622 Ratto, S., Abbruzzese, M., Abbruzzese, G., & Favale, E. (1983). Surface recording of the spinal
1623 ventral root discharge in man: An experimental study. *Brain*, *106*(4), 4.
1624 https://doi.org/10.1093/brain/106.4.897
1625 Reimann, A. F., & Anson, B. J. (1944). Vertebral level of termination of the spinal cord with report
1626 of a case of sacral cord. *The Anatomical Record*, *88*(1), 127–138.
1627 https://doi.org/10.1002/ar.1090880108
1628 Restuccia, D., Di Lazzaro, V., Valeriani, M., Conti, G., Tonali, P., & Mauguière, F. (1995). Origin
1629 and distribution of P13 and P14 far-field potentials after median nerve stimulation. Scalp,
1630 nasopharyngeal and neck recording in healthy subjects and in patients with cervical and

cervico-medullary lesions. *Electroencephalography and Clinical Neurophysiology/Evoked Potentials Section*, *96*(5), 5. https://doi.org/10.1016/0168-5597(95)00054-V

Rocchi, L., Suppa, A., Leodori, G., Celletti, C., Camerota, F., Rothwell, J., & Berardelli, A. (2018). Plasticity Induced in the Human Spinal Cord by Focal Muscle Vibration. *Frontiers in Neurology*, *9*, 935. https://doi.org/10.3389/fneur.2018.00935

Ruben, J., Krause, T., Taskin, B., Blankenburg, F., Moosmann, M., & Villringer, A. (2006). Subarea-specific Suppressive Interaction in the BOLD Responses to Simultaneous Finger Stimulation in Human Primary Somatosensory Cortex: Evidence for Increasing Rostral-to-caudal Convergence. *Cerebral Cortex*, *16*(6), 819–826. https://doi.org/10.1093/cercor/bhj025

Sandrini, G., Serrao, M., Rossi, P., Romaniello, A., Cruccu, G., & Willer, J. C. (2005). The lower limb flexion reflex in humans. *Progress in Neurobiology*, *77*(6), 353–395. https://doi.org/10.1016/j.pneurobio.2005.11.003

Satterthwaite, F. E. (1946). An Approximate Distribution of Estimates of Variance Components. *Biometrics Bulletin*, *2*(6), 110. https://doi.org/10.2307/3002019

Schieppati, M. (1987). The Hoffmann reflex: A means of assessing spinal reflex excitability and its descending control in man. *Progress in Neurobiology*, *28*(4), 345–376. https://doi.org/10.1016/0301-0082(87)90007-4

Severens, M., Farquhar, J., Desain, P., Duysens, J., & Gielen, C. (2010). Transient and steady-state responses to mechanical stimulation of different fingers reveal interactions based on lateral inhibition. *Clinical Neurophysiology*, *121*(12), 2090–2096. https://doi.org/10.1016/j.clinph.2010.05.016

1653 Shimoji, K. (1995). Origin and properties of spinal cord evoked potentials. In M. Dimitrijevic R.
1654 & J. Halter A. (Eds.), *Atlas of human spinal cord evoked potentials* (pp. 1–25).
1655 Butterworth-Heinemann.
1656 Shimoji, K., Kano, T., Higashi, H., Morioka, T., & Henschel, E. O. (1972). Evoked spinal
1657 electrograms recorded from epidural space in man. *Journal of Applied Physiology*, *33*(4),
1658 468–471. https://doi.org/10.1152/jappl.1972.33.4.468
1659 Stephani, T., Hodapp, A., Jamshidi Idaji, M., Villringer, A., & Nikulin, V. V. (2021). Neural
1660 excitability and sensory input determine intensity perception with opposing directions in
1661 initial cortical responses. *ELife*, *10*, e67838. https://doi.org/10.7554/eLife.67838
1662 Stephani, T., Nierula, B., Villringer, A., Eippert, F., & Nikulin, V. V. (2022). Cortical response
1663 variability is driven by local excitability changes with somatotopic organization.
1664 *NeuroImage*, *264*, 119687. https://doi.org/10.1016/j.neuroimage.2022.119687
1665 Stephani, T., Waterstraat, G., Haufe, S., Curio, G., Villringer, A., & Nikulin, V. V. (2020).
1666 Temporal Signatures of Criticality in Human Cortical Excitability as Probed by Early
1667 Somatosensory Responses. *The Journal of Neuroscience*, *40*(34), 6572–6583.
1668 https://doi.org/10.1523/JNEUROSCI.0241-20.2020
1669 Sumiya, S., Kawabata, S., Hoshino, Y., Adachi, Y., Sekihara, K., Tomizawa, S., Tomori, M., Ishii,
1670 S., Sakaki, K., Ukegawa, D., Ushio, S., Watanabe, T., & Okawa, A. (2017).
1671 Magnetospinography visualizes electrophysiological activity in the cervical spinal cord.
1672 *Scientific Reports*, *7*(1), 1. https://doi.org/10.1038/s41598-017-02406-8
1673 Suzuki, I., & Mayanagi, Y. (1984). Intracranial recording of short latency somatosensory evoked
1674 potentials in man: Identification of origin of each component. *Electroencephalography and*

Clinical Neurophysiology/Evoked Potentials Section, *59*(4), 286–296. https://doi.org/10.1016/0168-5597(84)90046-7

Synek, V. M. (1986a). Normative data for somatosensory evoked potentials from upper limb nerves in middle-aged subjects. *Clinical and Experimental Neurology*, *22*, 165–172.

Synek, V. M. (1986b). Somatosensory evoked potentials after stimulation of digital nerves in upper limbs: Normative data. *Electroencephalography and Clinical Neurophysiology/Evoked Potentials Section*, *65*(6), 6. https://doi.org/10.1016/0168-5597(86)90025-0

Tanosaki, M., Suzuki, A., Takino, R., Kimura, T., Iguchi, Y., Kurobe, Y., Haruta, Y., Hoshi, Y., & Hashimoto, I. (2002). Neural mechanisms for generation of tactile interference effects on somatosensory evoked magnetic fields in humans. *Clinical Neurophysiology*, *113*(5), 672–680. https://doi.org/10.1016/S1388-2457(02)00052-4

Tinazzi, M., & Mauguière, F. (1995). Assessment of intraspinal and intracranial conduction by P30 and P39 tibial nerve somatosensory evoked potentials in cervical cord, brainstem, and hemispheric lesions. *Journal of Clinical Neurophysiology: Official Publication of the American Electroencephalographic Society*, *12*(3), 237–253.

Tinazzi, M., Zanette, G., Bonato, C., Manganotti, P., Polo, A., Fiaschi, A., & Mauguière, F. (1996). Neural generators of tibial nerve P30 somatosensory evoked potential studied in patients with a focal lesion of the cervicomedullary junction. *Muscle & Nerve*, *19*(12), 1538–1548. https://doi.org/10.1002/(SICI)1097-4598(199612)19:12<1538::AID-MUS3>3.0.CO;2-B

Tinazzi, M., Zanette, G., Polo, A., Bonato, C., Manganotti, P., Fiaschi, A., & Mauguière, F. (1995). Subcortical P30 potential following tibial nerve stimulation: Detection and normative data. *The Italian Journal of Neurological Sciences*, *16*(8), 623–628. https://doi.org/10.1007/BF02230912

1698 Tsuji, S., Lüders, H., Lesser, R. P., Dinner, D. S., & Klem, G. (1984). Subcortical and cortical
1699 somatosensory potentials evoked by posterior tibial nerve stimulation: Normative values.
1700 *Electroencephalography and Clinical Neurophysiology/Evoked Potentials Section*, *59*(3),
1701 3. https://doi.org/10.1016/0168-5597(84)90061-3
1702 Turecek, J., Lehnert, B. P., & Ginty, D. D. (2022). *The encoding of touch by somatotopically*
1703 *aligned dorsal column subdivisions* [Preprint]. Neuroscience.
1704 https://doi.org/10.1101/2022.05.26.493601
1705 Waterstraat, G., Fedele, T., Burghoff, M., Scheer, H.-J., & Curio, G. (2015). Recording human
1706 cortical population spikes non-invasively – An EEG tutorial. *Journal of Neuroscience*
1707 *Methods*, *250*, 74–84. https://doi.org/10.1016/j.jneumeth.2014.08.013
1708 Ushio, S., Hoshino, Y., Kawabata, S., Adachi, Y., Sekihara, K., Sumiya, S., Ukegawa, D., Sakaki,
1709 K., Watanabe, T., Hasegawa, Y., & Okawa, A. (2019). Visualization of the electrical
1710 activity of the cauda equina using a magnetospinography system in healthy subjects.
1711 *Clinical Neurophysiology*, *130*(1), 1–11. https://doi.org/10.1016/j.clinph.2018.11.001
1712 Wheeler-Kingshott, C. A., Stroman, P. W., Schwab, J. M., Bacon, M., Bosma, R., Brooks, J.,
1713 Cadotte, D. W., Carlstedt, T., Ciccarelli, O., Cohen-Adad, J., Curt, A., Evangelou, N.,
1714 Fehlings, M. G., Filippi, M., Kelley, B. J., Kollias, S., Mackay, A., Porro, C. A., Smith, S.,
1715 … Tracey, I. (2014). The current state-of-the-art of spinal cord imaging: Applications.
1716 *NeuroImage*, *84*, 1082–1093. https://doi.org/10.1016/j.neuroimage.2013.07.014
1717 Willis, W. D., Weir, M. A., Skinner, R. D., & Bryan, R. N. (1973). Differential distribution of
1718 spinal cord field potentials. *Experimental Brain Research*, *17*(2).
1719 https://doi.org/10.1007/BF00235026

Yamada, T. (2000). Neuroanatomic substrates of lower extremity somatosensory evoked potentials. *Journal of Clinical Neurophysiology*, *17*(3), 269–279.

Yamada, T., Kimura, J., & Nitz, D. M. (1980). Short latency somatosensory evoked potentials following median nerve stimulation in man. *Electroencephalography and Clinical Neurophysiology*, *48*(4), 4. https://doi.org/10.1016/0013-4694(80)90129-7

Yamada, T., Machida, M., & Kimura, J. (1982). Far-field somatosensory evoked potentials after stimulation of the tibial nerve. *Neurology*, *32*(10), 10. https://doi.org/10.1212/WNL.32.10.1151

Yoshizawa, T., Nose, T., Moore, G. J., & Sillerud, L. O. (1996). Functional Magnetic Resonance Imaging of Motor Activation in the Human Cervical Spinal Cord. *NeuroImage*, *4*(3), 174–182. https://doi.org/10.1006/nimg.1996.0068

Supplementary material

I. Analysis differences between manuscript and preregistration

Experiment 1

- The preregistration stated that we aimed to also present SEPs at the channel with the strongest deflection. However, in the course of analyzing the data, we realized how well CCA was working on spinal data and decided that adding the time-course of the electrode with the strongest deflection would not bring additional value to the analysis, since CCA automatically incorporates the contribution of each channel to the SEP.

- The preregistration stated that we intended to investigate the relation between SEP amplitudes recorded at different levels of the somatosensory processing hierarchy. However, since we already show in Experiment 2 that there is mostly no such relation within one stimulation type, this analysis would not be very informative and we thus did not include it. Instead, we report a more informative analysis based on the data of Experiment 2, which allowed us to include different stimuli (i.e., mixed, single-digit and double-digit stimulation)

Experiment 2:

- In the preregistration we stated that we wanted to include brainstem and Erb's point potentials in our analysis. However, due to a low SNR we removed them from the results.

- The preregistration stated that we aimed to control for the difference in individual SEP latencies by taking the distance between the location of the recording and stimulation electrode into account. This was not necessary, because we used individual peak amplitudes and latencies in the present analysis.

- The preregistration stated that we intended to investigate the attenuation effect at the brainstem level (N14 and N30) as well. However, since the low SNR in the single-digit stimulation conditions did not allow for a observing clear SEPs at the brainstem level, we were not able not to perform this analysis.

- The preregistration stated that for testing attenuation effects, we aimed to test the summed single-digit SEP-amplitudes against the double-digit amplitudes with a paired t-test. Since in the literature it is however more typical to calculate individual interaction ratios, we followed this approach and tested them against zero (Hsieh et al., 1995; Severens et al., 2010). However, we also checked paired t-tests and saw that this did not change the statistical decision (i.e., significant and non-significant comparisons remained in both analysis).

II. Mixed nerve statistics from Experiment 2

Supplementary Table 1. *Group-level descriptive statistics for SEP- and NAP-amplitudes, latencies and SNR (mean and standard error of the mean) and one-sample t-test of SEP- and NAP-amplitudes in the hand-mixed and foot-mixed conditions of Experiment 2 (N = 24). Note that we only focused on the major peripheral, spinal and cortical components here for replication purposes and thus do not report Erb's point and brainstem potentials. Abbreviations: vr = ventral reference, tr = thoracic reference, CCA – canonical correlation analysis, SEP = somatosensory evoked potential, NAP = nerve action potential, # = number of participants in which potential was visible at the individual level, SNR = signal-to-noise ratio).*

SEP / NAP	#	Latency [ms]	Amplitude [µV / a.u.]	SNR	tstat	P	95%-CI	Cohen's d
Mixed median nerve stimulation (hand-mixed)								
N6	24	6.46 ± 0.10	-2.61 ± 0.29	36.52 ± 12.23	-8.93	<0.001	[-3.21; -2.01]	-1.82
N13 (tr)	24	13.46 ± 0.20	-0.86 ± 0.07	9.37 ± 1.51	-12.31	<0.001	[-1.01; -0.72]	-2.51
N13 (vr)	24	13.75 ± 0.17	-1.38 ± 0.09	14.36 ± 1.98	-16.09	<0.001	[-1.55; -1.20]	-3.28
N13 (CCA)	24	13.58 ± 0.19	-0.39 ± 0.04	24.01 ± 3.64	-10.40	<0.001	[-0.46; -0.31]	-2.12
N20 (CCA)	24	19.79 ± 0.17	-1.10 ± 0.08	24.07 ± 2.28	-13.80	<0.001	[-1.26; -0.93]	-2.82
Mixed tibial nerve stimulation (foot-mixed)								
N8	22	9.54 ± 0.16	-0.99 ± 0.16	13.30 ± 4.49	-6.20	<0.001	[-1.32; -0.66]	-1.27
N22 (tr)	24	24.21 ± 0.36	-0.57 ± 0.07	6.20 ± 1.07	-8.38	<0.001	[-0.71; -0.43]	-1.71
N22 (vr)	24	24.71 ± 0.43	-0.48 ± 0.06	10.09 ± 1.70	-8.53	<0.001	[-0.59; -0.36]	-1.74
N22 (CCA)	24	24.25 ± 0.32	-0.48 ± 0.05	24.97 ± 5.66	-9.46	<0.001	[-0.58; -0.37]	-1.93
P40 (CCA)	24	40.92 ± 0.58	1.17 ± 0.09	27.93 ± 3.07	12.80	<0.001	[0.98; 1.36]	2.62

III. Late potentials

Experiment 1:

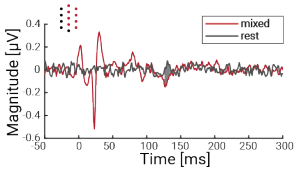

Supplementary Figure 1. *Grand-average over all participants in the foot-mixed condition and in simulated epochs from rest data. The plotted signal is an average over all channels that are part of the identified cluster (channels displayed as red dots on the top left). The gray area between 126-132 ms identifies the time range in which the two signals are statistically different; note that this result did not replicate in Experiment 2.*

Experiment 2: SEP components in the cervical and lumbar spinal cord that occur later than the N13 or the N22

We aimed to replicate the late potentials observed in Experiment 1 with the data from the mixed nerve conditions in Experiment 2, using an identical approach. The following responses were identified via cluster-based permutation testing (after the early potentials, which are ignored here): i) in the hand mixed condition, we identified a cervical cluster directly after the N13 component between 19 ms and 24 ms (p_{mcc} = 0.012; channels: S3, S6, S7, S9, S11, S14, S18) that has higher activity during stimulation than during rest and ii) in the foot-mixed condition, we identified a positive cluster directly after the N22 component between 29 ms and 35 ms (p_{mcc} = 0.004; channels: S22, S23, S26, L1, S28, S30, S32). This replicated the main results observed in Experiment 1, with the exception of the late potential displayed in Supplementary Figure 1.

IV. Effects of stimulation condition are shared across the somatosensory hierarchy

Experiment 2:

We here investigate whether response properties are shared across the somatosensory hierarchy and towards that aim compare the four different conditions presented in Experiment 2, which differ in the number and type of stimulated nerve fibers: while the mixed conditions stimulate all fibers of a nerve, the sensory conditions stimulate only parts of the sensory nerve fibers, which is consequently also reflected in the lower potential amplitudes. This allows us to investigate whether we can establish predictive links between the resulting potentials recorded at different levels of the

somatosensory processing hierarchy. To test this, we first took advantage of the possibility to extract single-trial cortical and spinal SEP amplitudes via CCA (as demonstrated above for the data from Experiment 1) and then examined the covariance of single-trial amplitudes of the neural responses along the somatosensory processing hierarchy with linear-mixed-effects (LME) models: peripheral NAPs were used to predict spinal SEPs and spinal SEPs were used to predict cortical SEPs, with the hypothesis of a positive relationship between potentials of the same direction and a negative relationship between potentials of opposite direction. LME models were fitted stepwise to the single-trial amplitudes, also including *stimulation condition* as a predictor (with the levels *mixed nerve*, *finger1/toe1*, *finger2/toe2*, *fingers1&2/toes1&2*).

Across the hand stimulation conditions, cortical SEP amplitudes were predicted by spinal SEP amplitudes, and spinal SEP amplitudes were predicted by peripheral NAP amplitudes ($\beta_{ESG} = 0.03$, $t(145171.5) = 10.01$, $p < 0.001$ and $\beta_{periphery} = 0.02$, $t(142032.7) = 8.40$, $p < 0.001$). Adding the factor *stimulation condition* to the models revealed that both these relationships were driven by effects of the type of stimulation on cortical SEP amplitudes ($\beta_{finger1} = 0.72$, $t_{finger1}(145163.8) = 98.35$, $\beta_{finger2} = 0.62$, $t_{finger2}(145185.0) = 89.15$, $\beta_{fingers1\&2} = 0.47$, $t_{fingers1\&2}(145185.0) = 66.99$, all $p < 0.001$), as well as on spinal SEP amplitudes ($\beta_{finger1} = 0.21$, $t_{finger1}(136741.6) = 26.11$, $\beta_{finger2} = 0.19$, $t_{finger2}(141498.6) = 24.22$, $\beta_{fingers1\&2} = 0.15$, $t_{fingers1\&2}(141288.6) = 19.87$, all $p < 0.001$); effect contrasts with reference level *mixed nerve stimulation*. At the same time, the effects of spinal SEP on cortical SEP amplitude and of peripheral NAP amplitude on spinal SEP amplitude were no longer significant and thus fully explained by *stimulation condition* ($\beta_{ESG} = 0.001$, $t(145177.4) = 0.72$, $p = 0.47$ and $\beta_{periphery} = -0.00$, $t(142364.2) = -0.42$, $p = 0.672$). Hence, *finger1*, *finger2*, as well as *fingers1&2* stimulations all resulted in differential amplitudes as compared to *mixed nerve* stimulation, both on the spinal as well as on the cortical level, and this amplitude variance was fully shared among the processing levels, explaining single-trial covariation across periphery, spinal cord and cortex.

A similar picture emerged for foot stimuli: cortical SEP amplitudes were predicted by spinal SEP amplitudes ($\beta_{ESG} = -0.04$, $t(151307.0) = -14.38$, $p < 0.001$) and spinal SEP amplitudes were predicted by peripheral NAP amplitudes ($\beta_{periphery} = 0.02$, $t(151223.8) = 7.94$, $p < 0.001$) when not controlling for stimulation conditions; please note that the negative sign of β_{ESG} reflects the fact that spinal SEP amplitudes are measured as negative potentials while the first cortical SEP in the foot region, the P40, is a positive peak. When adding the factor *stimulation condition*, again, all types of stimulation affected the cortical level ($\beta_{toe1} = -0.61$, $t_{toe\ 1}(151264.6) = -86.60$, $\beta_{toe2} = -0.50$, $t_{toe2}(151264.8) = -70.15$, $\beta_{toes1\&2} = -0.32$, $t_{toes1\&2}(151268.8) = -46.32$, all $p < 0.001$) as well as the spinal level ($\beta_{toe1} = 0.33$, $t_{toe\ 1}(140802.2) = 43.82$, $\beta_{toe2} = 0.33$, $t_{toe2}(140806.3) = 43.51$, $\beta_{toes1\&2} = .26$, $t_{toes1\&2}(141379.1) = 35.86$, all $p < 0.001$). While the factor *stimulation condition* fully accounted for the effect of peripheral NAP on spinal amplitude, which was no longer existent ($\beta_{periphery} = 0.00$, $t(151323.8) = 0.00$, $p > 0.99$), a main – though slightly attenuated – effect of spinal amplitude on cortical amplitude still remained ($\beta_{ESG} = -0.02$, $t(151320.4) = -3.72$, $p < 0.001$). Additionally, small interaction effects on cortical amplitudes emerged between spinal amplitudes and toe2 stimulation, $\beta_{ESG * toe\ 2} = 0.02$, $t_{\ ESG * toe2}(151314.1) = 3.02$, $p_{ESG * toe2} = 0.003$, as well as between spinal amplitudes and toes 1 & 2 stimulation, $\beta_{ESG * toes1\&2} = 0.02$, $t_{\ ESG * toes1\&2}(151314.5) = 2.99$, $p_{ESG * toes1\&2} = 0.003$.

Taken together, the effects of different stimulation types (i.e., *mixed nerve, finger1/toe1*, *finger2/toe2*, *fingers1&2/toes1&2*) seem to propagate through the somatosensory processing hierarchy, jointly affecting the amplitudes of peripheral NAPs, spinal cord responses, and initial cortical potentials in the primary somatosensory cortex. This observation applied to both hand and foot stimulation, though with additional effects of spinal amplitudes on cortical amplitudes beyond the effect of stimulation condition in foot stimuli.